Lehigh University
Lehigh Preserve

Theses and Dissertations

2015

The Effect of a Passivation Layer on the Anelastic Response of Gold Thin Films

Patrick Holmes
Lehigh University

Follow this and additional works at: http://preserve.lehigh.edu/etd

Part of the Materials Science and Engineering Commons

Recommended Citation
Holmes, Patrick, "The Effect of a Passivation Layer on the Anelastic Response of Gold Thin Films" (2015). *Theses and Dissertations*. 2636.
http://preserve.lehigh.edu/etd/2636

This Thesis is brought to you for free and open access by Lehigh Preserve. It has been accepted for inclusion in Theses and Dissertations by an authorized administrator of Lehigh Preserve. For more information, please contact preserve@lehigh.edu.

The Effect of a Passivation Layer on the Anelastic Response of Gold Thin Films

by

Patrick M. Holmes

Presented to the Graduate and Research Committee of Lehigh University in Candidacy
for the Degree of Master of Science

in
Materials Science and Engineering

Lehigh University
May 2015

© Copyright 2015 by Patrick Michael Holmes
All Rights Reserved

This thesis is accepted and approved in partial fulfillment of the requirements for the Master of Science.

____
Date

____
Dr. Richard P. Vinci
Thesis Advisor

____
Dr. Helen M. Chan
Department Chairperson

Acknowledgements

First and foremost I wish to thank all of those in the department who have helped me reach where I am today. My deepest gratitude goes out to Dr. Richard P. Vinci for his patience and understanding throughout my years as both an undergrad and a graduate student. Without his guidance, I would not have been able to reach any level close to where I am now. I especially wish to thank Walter L. Brown for his help and explanations throughout my work presented in this thesis. Without his teaching about the bulge test stand, I would still be lost. Additional thanks must also be given to Jeff Smyth, who kept me from getting too discouraged during the countless instances of setbacks or delays due to bulge misbehavior - as if the system was aware of what I was trying to do. Ling Ju and Rod Marstell also deserve thanks for their aid helping me use the ALD equipment to coat my films. This work could not have reached fruition without any of those mentioned above. I also wish to thank my family for keeping me motivated when work was slow and full of delays.

To my other friends in the department: thank you for keeping things light. I truly appreciated the humor and camaraderie between advisor groups. Without you all my time as a graduate student would have felt much longer. You all have been great friends and coworkers during my time here.

Table of Contents

Acknowledgements……………………………………………………………………iv

List of Figures…………………………………………………………………………vii

Abstract……………………………………………………………………………… 1

1. Introduction and Background…………………………………………………….... 2

 1.1. Introduction……………………………………………………………………….2

 1.2. Background……………………………………………………………………….3

  1.2.1. Evolution of MEMS…………………………………………………………….3

  1.2.2. Radio Frequency MEMS………………………………………………………. 4

  1.2.3. Mechanical behavior of thin films……………………………………….... 6

  1.2.4. Anelasticity…………………………………………………………………….. 7

  1.2.5. Stress relaxation related reliability issues………………………………… 9

  1.2.6. Mechanical testing methods for thin film materials………..…………... 11

  1.2.7. Common theories of time-dependent deformation in metal thin films…..13

  1.2.8. Material parameters affecting viscoelastic response in metal thin films... 14

  1.2.9. Outline of this thesis…………………………………………………….. 17

2. Experimental Procedure……………………………………………………………...17

 2.1. Sample design and fabrication…………………………………………………..17

 2.2. Fabrication of Au films and surface treatments…………………………………19

 2.3. Bulge testing………………………………………………………………………21

  2.3.1. Bulge measurement technique…………………………………………... 21

  2.3.2. Stress relaxation experiments…………………………………………… 27

3. Results and Discussion………………………………………………………………… 29

3.1. Iso-strain conditions for pure gold………………………………………………29

3.2. Iso-strain conditions for uncoated sample………………………………………31

3.3. Iso-strain conditions for ALD coated samples…………………………………..33

3.4. Iso-strain conditions for film on SiN_x substrate………………………………....40

3.5. Iso-strain conditions with 20nm TiO_2…………………………………………...42

3.6. Theories for comparable iso-strain behavior of tests……………………………45

3.6.1. Ti passivation layer……………………………………………………… 45

3.6.2. Grain boundary sliding…..………………………………………………..49

3.6.3. Dislocation based mechanism……………………………………………49

3.7. Dislocation mobility in films…………………………………………………… 53

4. Summary and Conclusions...54

5. References………………………………………………………………………58

6. Vita……………………………………………………………………………...62

List of Figures

Figure 1.1 MEMS deformable mirror (a) showing the mirror segments attached to thin springs. Underneath the mirrors are actuators that alter the mirrors positions [1], and (b) active structure of a 3D gyroscope [2]……………………………………………………4

Figure 1.2 Top view of a RF MEMS capacitive switch. The bowtie shape is a thin film metal membrane which is clamped at either end and is deflected downward by electrostatic force to close the switch………………………………………………….. 6

Figure. 1.3 Open and closed states of RF MEMS capacitive switches ……………….......6

Figure 1.4 Elastic, plastic and anelastic behavior in materials…………………………… 8

Figure 2.1 a) Bulge sample bottom view, and (b) cross section view…………………... 18

Figure 2.2 Steps of Sample Fabrication for Bulge Testing………………………………19

Figure 2.3 Au films under identical sputtering conditions with testing procedures…….. 21

Figure 2.4 Method of bulge test with known geometrical parameters………………….. 22

Figure 2.5 Electrical setup of bulge test…………………………………………………23

Figure 2.6 Example of 4 term polynomial fit function to describe the relationship between C and bulge height……………………………………………………………………. 26

Figure 2.7 Typical pressure ramp to determine plane strain modulus and residual stress in films…………………………………………………………………………………... 28

Figure 3.1 Normalized modulus iso-strain curves for pure freestanding gold………….. 30

Figure 3.2 Modulus and residual stress changes in pure Au film throughout testing cycles……………………………………………………………………………………..31

Figure 3.3 Normalized modulus iso-strain curves for freestanding uncoated Au on Titanium…………………………………………………………………………….32

Figure 3.4 Modulus and residual stress changes in uncoated Au on Ti film throughout testing cycles…………………………………………………………………………..33

Figure 3.5 Normalized modulus iso-strain curves for freestanding Au on Ti coated with passivation layer immediately after film sputtering…………………..……………….34

Figure 3.6 Modulus and residual stress changes throughout testing cycles of Au on Ti films subjected to passivation immediately after sputtering……………………………..35

Figure 3.7 Normalized modulus of iso-strain curves for coated Au on Ti. Passivation layer was deposited 2 weeks after initial sputtering…………………………………….. 36

Figure 3.8 Normalized modulus of iso-strain curves for ALD coated Au on Ti. Passivation layer was deposited after uncoated sample had reached steady state conditions……………………………………………………………………………...36

Figure 3.9 Modulus and residual stress changes throughout testing cycles of Au on Ti films subjected to passivation immediately after sputtering……………………………..37

Figure 3.10 Modulus and residual stress changes throughout testing cycles of Au on Ti films subjected to passivation 2 weeks after sputtering………………………………….38

Figure 3.11 Modulus and residual stress changes throughout testing cycles of Au on Ti films subjected to passivation after uncoated sample reached steady state conditions…. 38

Figure 3.12 Initial stress relaxation behavior of tests…………………………………… 39

Figure 3.13 Steady state behavior of all tests…………………………………………… 40

Figure 3.14 Normalized modulus of iso-strain curves for coated Au/Ti on SiN_x………..41

Figure 3.15 Normalized modulus of iso-strain curves for 20nm of TiO_2 on Au/Ti film……………………………………………………………………………………43

Figure 3.16 Initial stress relaxation behavior for tested samples………………………...43

Figure 3.17 Steady state behavior for all tested sample…………………………………44

Figure 3.18 Schematic portraying titanium diffusion to the surface via the grain boundaries……………………………………………………………………………….. 46

Figure 3.19Au/Ti film LEIS analysis showing presence of atoms on the surface, one monolayer deep, and 2 monolayers deep…………………………………………………...48

Figure 3.20 Depth profile showing a plateau of gold signal with depth…………………48

Figure 3.21 Characteristic steady state conditions at room temperature for a thin film……………………………………………………………………………………….50

Figure 3.22 Dislocation motion without ALD coatings and with ALD coatings……….. 51

Figure 3.23 a) Plot of stress response of a material when heated past the elastic temperature limit results in an increase in residual stress results from cooling, and b) a comparison to Lin's cantilever behavior – reproduced from [41]……………………………………..52

Figure 3.24 a) A dislocation segment is pinned a two points in the same Peierls energy trough, b) applying a stress causes a segment of the dislocation to advance through the Peierls potential and create a double kink……………………………………………..54

Abstract

The anelastic response in 500nm Au films has been studied through stress relaxation measurements using gas pressure bulge testing under iso-strain conditions. Samples were subjected to various processing techniques before testing to determine if these parameters affected steady state behavior of films. Stress relaxation experiments consisted of a rapid pressure ramp from zero strain to an applied strain of 0.1% and held for 3 hours. A series of such tests were conducted on each sample, one per day, to allow for any viscoelastic stress recovery.

Stress relaxation consisted of two components: a fully recoverable viscoelastic component and a non-recoverable plastic (creep) component. The non-recoverable component decreased to zero after a series of three hour iso-strain tests, until a steady state was reached with purely a viscoelastic component remaining. By varying surface conditions on the film (passivation layer presence, titanium adhesive layers, SiN_x substrate layers), it was concluded that at these temperatures and testing conditions result in a dislocation based mechanism for deformation rather than a surface and grain boundary diffusion based mechanism seen in other work. Dislocation double-kink nucleation is proposed as a possible mechanism for relaxation.

1. Introduction and Background

1.1 Introduction

Devices utilizing metal thin films are continuously growing in number throughout a wide range of engineering applications. Of particular interest for the present work is the application called MicroElectroMichanical Systems (MEMS). Many MEMS devices use silicon as an electrical, mechanical, or optical element; but there are certain applications for which silicon has inadequate electrical conductivity or optical reflectivity. For these applications, metal films are often required. Although metal films generally have attractive electrical and optical properties, they also suffer from certain mechanical shortcomings that are not ideal for a MEMS device. The small-scale nature of thin films brings about a new regime of material properties that often are quite different from behavior of bulk materials. For example, it is often the case that the strength of a thin metal film is greater than that of its bulk counterpart, but toughness is often lower. Much work has been devoted to characterizing thin metal film mechanical properties, but the phenomenon of anelasticity (also known as viscoelasticity) has been given relatively little attention and must be better understood because it can have a significant effect on MEMS performance and reliability. This thesis presents work that will contribute to understanding the anelastic response in gold films subjected to a variety of interface conditions. Anelastic response is observed via stress relaxation measurements performed by bulge testing. Key goals of this work are to determine which interface conditions — if any — can reduce or eliminate anelastic behavior, and in doing so to determine whether

the mechanisms responsible for anelastic stress relaxation are the same mechanisms responsible for more commonly studied relaxation phenomena.

1.2 Background

1.2.1 Evolution of MEMS

In itself, the development of integrated circuits is a remarkable advancement for the information era. Ultimately every corner of manufacturing, business, telecommunications, and transportation systems utilize computers and thus depend on the functionality and reliability of the integrated circuit. Integrated circuits heavily depend on, and extensively use, thin film materials. Modern microprocessors contain millions of transistors; each of which requiring thin films to function. This translates to many hundreds of meters of thin metal wires used in interconnects within each microprocessor.

The next evolutionary step in integrated circuits is the marriage of electrical components with mechanical components within a very confined space. Integrated circuit processing techniques allow for a very refined and tight combination of electrical and mechanical components. This arrangement is the crucial stepping stone for development of sensors and actuators with very small sizes, low costs, and better performances to conventional alternatives. These micro-electrical-mechanical devices (MEMS) are used in gyroscopes, optical displays, pressure sensors, biomedical devices and electronic switches. Sizes of these devices can range from several mm down to several hundred nm. Examples of some MEMS devices are shown in Fig. 1.1 [1, 2] Of particular interest for this study is a type of MEMS device which can be mechanically manipulated to alter radio-frequency (RF) signal paths.

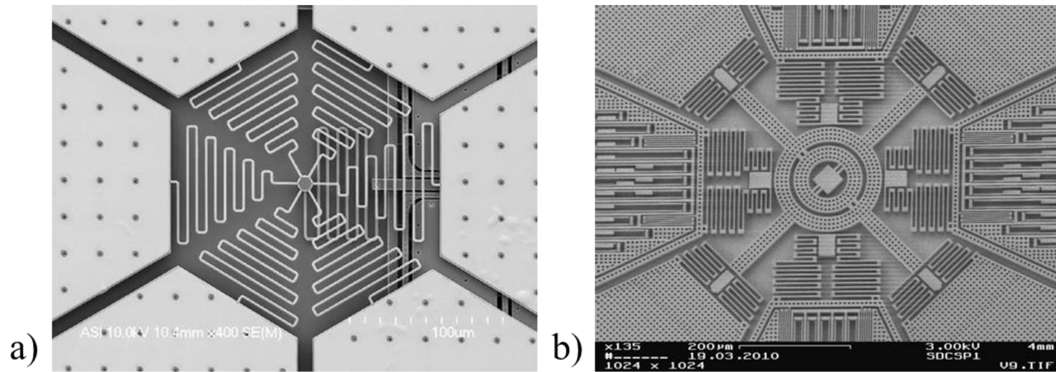

Figure 1.1. MEMS deformable mirror (a) showing the mirror segments attached to thin springs. Underneath the mirrors are actuators that alter the mirrors positions [1], and (b) active structure of a 3D gyroscope [2].

1.2.2 Radio frequency MEMS

Radio frequency (RF) MEMS devices often utilize a suspended membrane or a freestanding cantilever in their construction. They make use of mechanical movement of the membrane or cantilever to open and close electrical circuits and thus act as a switch. This mechanical movement can be attained by thermal, piezoelectric, magnetostatic or electrostatic actuation. Of interest to this study is electrostatic actuation of RF capacitive MEMS. The main areas of application for these types of switches include: Radar Systems for Defense Applications (5-94 GHz), Automotive Radars (24, 60 and 77 GHz), Satellite Communication Systems (12-35 GHz) and Wireless Communication Systems (0.8-6 GHz) [3]. There are several advantages that accompany this application such as: reduced weight due to smaller size, little power consumption, high linearity, low insertion loss and lower cost than solid state switches [4].

A typical RF MEMS device can be seen in Fig 2. This switch actuates through attractive forces resulting from a charge applied to a lower electrode under the movable

film or cantilever. When the lower plate has no charge, the membrane is flat and the RF signal is transported from end to end. However, when a voltage is applied to the lower electrode, the membrane is pulled down to just above or in contact with the electrode. This "down" state shorts the RF signal to ground and no signal flows along the transmission line. The membrane is under tension while the pull-down voltage is on. Once the voltage is turned off on the stationary electrode, under ideal conditions the elastic energy in the stressed film pulls the membrane back to zero strain, separating it from the electrode. This opens the switch, allowing the RF signal to flow. Electronically speaking, RF MEMS switches can either function in a capacitive or metal-contact method. The difference between these two switch types is the presence or absence of a dielectric layer on top of the stationary electrode. For a capacitive switch, the film contacts the dielectric but never the metal pad beneath the dielectric. Signal is able to travel through the dielectric pad to ground and be diverted. In a metal-contact switch, the membrane directly touches a metal pad to ground to divert any signal. This process can be seen in Fig 3.

When compared to solid state diode-based switches, capacitive MEMS switches have several distinct advantages. In addition to FETs and PIN diodes, there are many advantages RF switches have over conventional electromagnetic relays. These include: smaller size, lower power consumption, greater reliability (billions - hundreds of billion cycles), lower cost, and better performance [5]. However, some disadvantages include: environment sensitivity, lack of capability to handle high power, and greater isolation requirements [5].

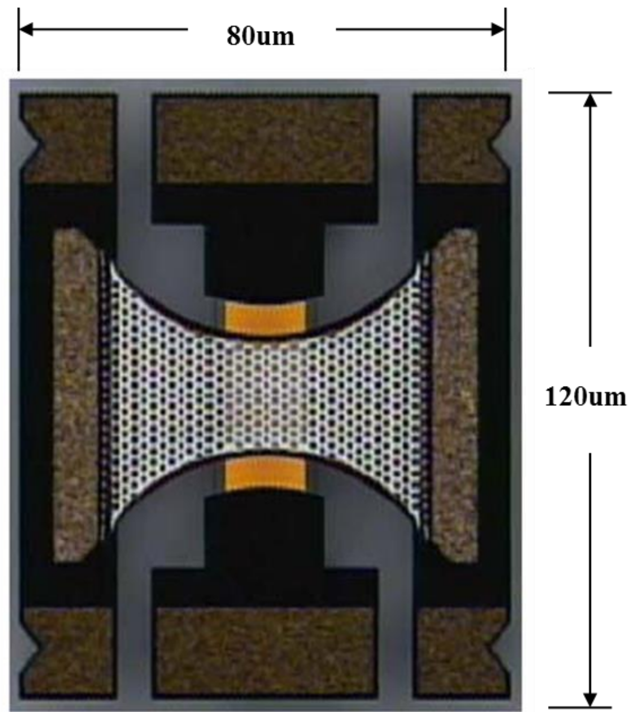

Figure 1.2 Top view of a RF MEMS capacitive switch. The bowtie shape is a thin film metal membrane which is clamped at either end and is deflected downward by electrostatic force to close the switch

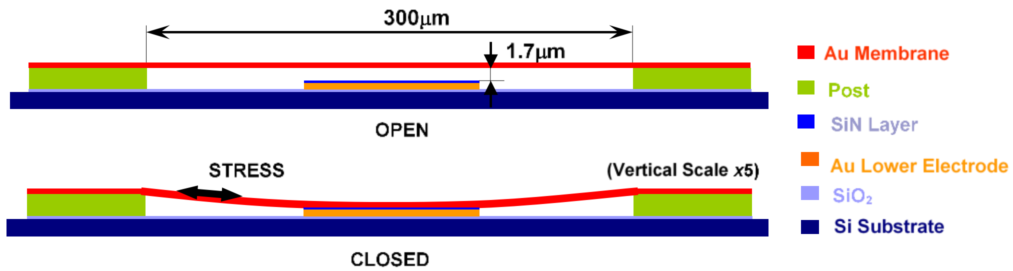

Figure 1.3 Open and closed states of RF MEMS capacitive switches

1.2.3 Mechanical behavior of thin films

For RF MEMS and other types of MEMS, thin films can act as components that carry loads. These could be mechanical, such as hinges or springs in micro-mirrors, or

electrostatic, such as in RF MEMS. In either case, it is ideal to have a constant displacement for a given applied force to the beam, cantilever, or spring. It is therefore critical for development and manufacturing of these devices to understand how the films will behave over time. Thin film properties with the greatest influence on the lifetime and behavior of these devices are the residual stress, elastic/plastic behavior, anelastic behavior and fatigue.

Thin films are fabricated in a very different method from their bulk counterparts. Methods of fabrication include epitaxial growth, chemical vapor deposition, and physical vapor deposition processes. These processes very often result in residual stress in the films due to thermal expansion mismatch of the substrate and the film [6]. Residual stresses can be adjusted by altering substrate deposition temperatures during fabrication or post fabrication thermal cycling.

1.2.4 Anelasticity

Anelastic behavior is inherently different from either an elastic or plastic response. This behavior is very commonly found in polymers and in thin metal films [7-9] where there is time dependent deformation as well as recoverable response once constraints are removed. When an elastic strain is imposed, the elastic modulus is simply defined through Hooke's Law as $E = \sigma/\varepsilon$. For a purely elastic case such as this (Fig 1.4 a), a constant applied strain generates a constant state of stress, yielding a time independent modulus and a lack of deformation once the strain is reversed. In the case of time dependent plasticity, a material under a constant strain shows a time dependent reduction in stress followed by permanent deformation when the strain is reversed, Fig.

1.4 b. An anelastic response shows time dependent deformation without any permanent deformation, Fig. 1.4 c. In this case, the behavior can be modeled as a time-dependent elastic modulus, E(t) = σ(t)/ε.

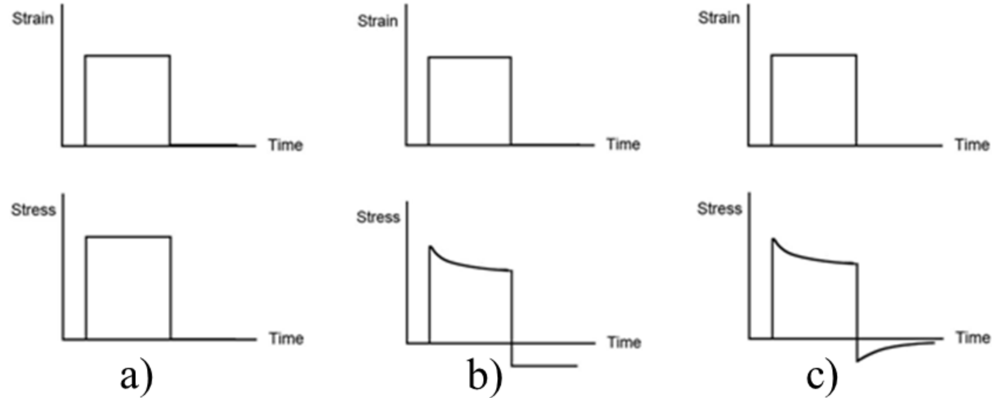

Figure 1.4 Elastic, plastic and anelastic behavior in materials

In the case of linear anelasticity, the time dependent elastic modulus is independent of the magnitude of stress and strain. It has been shown by Hyun et al. that thin metal films display a linear viscoelastic response to applied loads [10]. A linear elastic model can then be used to demonstrate the stress vs. time behavior dependent on strain history [11]:

$$\sigma(t) = \sigma_0 + \varepsilon_o E(t) + \int_0^t E(t-\xi)\frac{d\varepsilon(\xi)}{d\xi}d\xi \qquad (1.1)$$

where σ_0 is the residual stress in the material, ε_0 is the instantaneous applied strain and $d\varepsilon(\xi)/d\xi$ is the strain rate. The time dependent modulus can therefore be expressed as a Prony series of saturating exponentials [12]:

$$E(t) = E_0\left(1 - \sum_{i=1}^{n} p_i (1 - e^{-t/\tau_i})\right) \quad (1.2)$$

where E_0 is the instantaneous modulus and τ_i is the i*th* time constant. The time dependent modulus must obey the following rules:

$$E_0 \geq 0,\ p_i \geq 0, \sum_i p_i \leq 1, \tau_i \geq 0 \quad (1.3)$$

Hyun et al. observed linear anelasticity in 1.16 um thick Al films. Using the bulge test, they determined time-dependent stress recovery behavior following stress relaxation. Also studied was change in stress relaxation due to different strain rates.

1.2.5 Stress relaxation related reliability issues in RF MEMS capacitive switches

Anelastic behavior of thin films is of crucial significance when attempting to lengthen the life of capacitive RF MEMS switches. There are typically two modes of operation for RF MEMS switches: the switch can be held open or closed for extended periods of time or it can cyclically be switched on and off at frequencies on the range of kilohertz or higher. In either mode of operation, if stress in the metal membrane relaxes with time while it is in the actuated state, the internal restoring force necessary for the film to return to zero stress will also decrease and the film will no lnger be flat when relased. These changes cause two failure modes: stiction and a change in pull-down voltage.

The reduction in restoring force associated with stress relaxation can lead to catastrophic stiction, a typical failure mechanism where the membrane and dielectric

layer do not separate after the actuation voltage is turned off [13-14]. Once stiction occurs, the membrane restoring force will continue to decrease and permanent failure will occur.

The actuation voltage required to close a switch is often as large as 40 V. It has been shown that the dielectric layer can retain trapped charges built up over time which slowly bleeds out after the voltage is removed [15]. This excess trapped charge creates an unintended attractive electrostatic force between the film and the dielectric. Over time, the restoring force in the film must continue to be high enough to overcome this trapping phenomenon. As switch cycles increase, so too does the amount of trapped charge in the dielectric layer and eventually the film's intrinsic restoring force is not enough to overcome the electrostatic force. Once this occurs, the switch will fail in the down position. This effect can occur more quickly if stress relaxation within the film is present.

Even if the stiction forces can be overcome, the stress relaxation that occurs in the down state leads to viscoelastic strain. This strain is manifested in a temporary change in the length of the membrane so that it fails to return instantaneously to its original flat shape. The gap between the film and the lower electrode is reduced and the film tends to pull down at lower voltage on the next actuation cycle. If severe, this is also considered a failure mode because the device is not operating according to the design parameters.

Yan et al. observed both viscoelastic and viscoplastic stress relaxation in thin metal films [16]. The underlying difference between these types of time dependent behavior is that viscoplastic relaxation is not recoverable while viscoelastic behavior is. The degree of viscoplasticity also has been shown to decrease with time, whereas the

viscoelastic contribution is continuously present. As the lifetime of the switch extends, the viscoplastic dependence will diminish to a negligible level, while viscoelasticity will continue to be present. Previous work has shown that Au films and cantilevers with typical RF MEMS film thicknesses (1-1.2 um) display both an anelastic response and creep behavior [9, 17]. Each of these will reduce the restoring force in the Au film.

1.2.6 Mechanical testing methods for thin film materials

Several commonly used methods have been developed for measuring time-dependent mechanical properties of thin films. A developing technique is measuring creep compliance of viscoelastic materials via nano-indentation [18-20]. In this method, two types of indenting can be utilized. In each, a nano-indenting tip is brought in contact with the surface of a material. Either indent depth as a function of time under constant force is recorded or force as a function of time under constant strain is measured. The benefit of this technique is that any material can be tested (provided an adequately smooth surface) and the area of interest is very small. Hardness, elastic modulus, residual stress, fracture toughness and viscoelastic behavior can all be determined via nano-indentation. Drawbacks that must be considered are the stress state under the indenter is triaxial and thermal drift must also be accounted for over extended time periods.

Another technique widely used is the wafer curvature measurement [17,21-22]. In this type of experiment, the curvature of a film on a substrate is measured and then related to stress in the film by the Stoney equation [23]. Due to thermal mismatch between a thin film and the substrate, changes in temperature directly contribute to variations in stress between the film and substrate, causing the assembly to develop

curvature. The curvature of the substrate typically is evaluated by white light interferometry or lasers [17]. The Stoney equation relates the stress to the difference in radii of the substrate with and without a film:

$$\boldsymbol{\sigma} = \frac{M_s t_s^2}{6t_f}\left(\frac{1}{R_1} - \frac{1}{R_2}\right) \quad (1.4)$$

where t_f is the film thickness, t_s is the substrate thickness, M_s is elastic biaxial modulus of the substrate, R_1 is spherical radius of curvature of the composite film/substrate neutral plane, R_2 is the spherical radius of curvature of the bare substrate mid-plane/neutral plane, and σ is the biaxial stress in the thin film. Both sample fabrication and measurement techniques are simple and this method can work with any type of film. However, the presence of a substrate can alter the mechanical properties of thin films. It has been shown that the presence of a substrate or a passivation layer can influence both plastic [24] and anelastic [22, 25] behavior of metal films.

The largest reason for this discrepancy from freestanding films is that passivation layers and substrates both constrain dislocation motion in films by pinning dislocations and preventing any annihilation at a free surface. This creates back stresses and causes the flow stress and yield stress to increase while at the same time reducing dislocation-based relaxation mechanisms.

A third technique used for time-dependent thin film mechanical testing is microtensile testing [26-28]. This method requires use of an actuator with nanometer displacement control. Most often, piezoelectrics are used in these devices for their electronic sensitivity. The actuator applies a tensile load to a thin film and records the displacement and force, which can then be transferred to stress and strain [29]. The

benefit of this method is the ability to perform tests on freestanding films and eliminating substrate effects. Difficulties tend to arise during sample mounting and alignment.

In this study, we employ a fourth method utilizing the thin film bulge method [8-10, 16, 30-31]. Applying a gas pressure differential across a thin film membrane allows for determination of Young's Modulus and tensile residual stress. In this setup, samples are created via standard semiconductor fabrication technique to create a freestanding rectangular thin film membrane with known geometry etched out of a substrate. The pressure differential across the membrane due to added gas on one side forces the membrane to deform elastically. Measurements of pressure and bulge height can be converted to stress and strain, respectively. The height of the bulge can be determined in several ways including light interferometry [30] or by capacitance measurements [8-10]. Advantages of bulge testing techniques include measurements of freestanding films without the difficulties of sample mounting and alignment that are common in tensile methods, and also the ability to independently apply a temperature change and a strain change.

1.2.7 Common theories of time-dependent deformation in metal thin films

The most accepted time-dependent deformation mechanism theory is grain boundary diffusion [21-22] due to the fact that grain boundaries act as diffusion short circuits in metals [31-33] and thus have a faster flow of vacancies/atoms than bulk diffusion. Thin films are noticeably susceptible to grain boundary diffusion due to small grain size and a larger volume fraction of boundaries (compared to bulk metals). Coble

creep is more sensitive to grain size than Nabarro-Herring creep, suggesting that Coble creep will dominate the creep rate in very fine grained materials [35-36]

Another proposed viscoelastic mechanism is obstacle controlled dislocation glide, where dislocation motion is hindered by obstacles such as other dislocations, grain boundaries, solute atoms, or precipitates [37]. The degree of strengthening depends on the energy needed to overcome the obstacles without aid from external stress. If a dislocation is pinned by these obstacles, under applied stress the dislocation will bow out and create a radius of curvature. As the stress is removed (time dependent) the bowed out dislocation will return to its original shape.

A third viscoelastic mechanism is grain boundary sliding, where under an applied load, shear stresses across boundaries cause the grains to slip past each other [38-39]. It should be noted that without bulk and grain boundary diffusion, voids at triple points would nucleate due to sliding. This process this therefore coupled with diffusion processes to conserve volume.

1.2.8 Material parameters affecting viscoelastic response in metal thin films

Time dependent deformation can be divided into two regimes: viscoplastic and viscoelastic. The first describes time dependent permanent deformation under an applied load. Viscoplasticity is similar to creep [3,17,19]. The latter describes time dependent deformation that gradually disappears when the load is removed. The viscoelasticity phenomenon is perpetually present in thin metal films, whereas the capacity for viscoplasticity decreases over time until its contribution is negligible.

One method to attempt to reduce permanent time-dependent deformation is to add an oxide passivation layer [22-23,40]. In a typical unpassivated thin film, surface diffusion can enable stress relaxation through the formation of grain boundary grooves. In addition, applied stresses promote nucleation and motion of dislocations that may move to the surface and annihilate. Adding a passivation layer reduces surface diffusion and can prevent the formation of steps at the surface; thereby hindering dislocation surface annihilation. Dislocations pile up at the interface and create back stresses on the sources [24,40-41]. This passivation layer reduces the effect of viscoplasticity as well as viscoelasticity by increasing the back stress on dislocation sources until they can no longer emit a dislocation [24]. This in turn limits amount of deformation under an applied strain. Shen et al. also noticed a significant degree of stress relaxation at high temperatures for unpassivated thin Cu films. Yet passivated Cu films did not exhibit significant stress relaxation at these temperatures. They attributed this fact to the prevention of surface atomic diffusion from relaxing the stress and the constrained dislocation motion due to the passivation.

In addition to passivation and temperature effects, gain size also has been seen to play a role in viscoelastic/viscoplastic response of thin films [42-43]. In these cases, grain boundaries and surfaces controlled material creep at room temperature. In Gall et al. [17], they examined the thermomechanics of creep in thin Au film on curved bimaterial Au/Si microcantilevers. By measuring curvature of the microcantilevers over time, they determined time-dependent inelastic strains in Au films. They concluded that inelastic

behavior in thin films is dependent on annealing temperature, grain size, film stress, and degree of passivation.

Lin et al. [41] further examined the effect a passivation layer has on stress relaxation in gold films by measuring changes in curvature of Au-Si microcantilevers. Using differences in thermal expansion coefficients between gold and Si, Lin was able to quantify the relative temperature dependence of residual stress in a film upon heating with and without the presence of an atomic layer deposition (ALD) layer of aluminum oxide. They determined that adding ALD coatings to films greatly reduces the change in film residual stress that occur when the film is heated between 20-200°C.

Lin also ran isothermal tests at elevated temperatures for 60 hours to determine the degree of stress reduction with time. Increasing passivation layer thickness on the metal films greatly reduced the degree of stress relaxation seen. However, this testing style results in non-equilibrium stress relaxation; meaning the degree of relaxation is dependent on the current film stress and strain. In this case, as the film relaxes, it changes shape. This shape change then causes the driving force for stress related atomic diffusion to go down. This procedure for testing stress relaxation may induce different mechanisms for deformation than an iso-strain stress relaxation test. For iso-strain tests, the film is in a state of equilibrium and will not change shape, nor will the degree of stress relaxation depend on current stress in the film.

The positive effects of an ALD layer on the stress relaxation of gold thin films is very encouraging but there are limitation to the Lin study that motivate additional investigation. First, Lin et al. induced strain thermally so they were not able to separate

temperature effects from strain effects. Second, the temperatures at which the relaxation occurred were fairly high for a MEMS device: typically well over 100 C. Finally, the isothermal stress relaxation was not separated into viscoplastic and viscoelastic components so it is not known if the ALD layer affected both phenomena.

1.2.9 Outline of this thesis:

In the following chapters, viscoelastic stress relaxation and changes in viscoplasticity are measured using gas pressure bulge testing at typical switch operating temperature (20°C). The effects of passivation layer on the degree of viscoplasticity is compared between specimens. Initial stress relaxation behavior and steady state relaxation behavior are also compared between tests in an effort to better understand the long term behavior of thin film capacitive/metal contact RF MEMS switches.

2. Experimental Procedure

2.1 Sample design and fabrication

For gas bulge testing, specimens consisted of a thin film with known thickness suspended over a 12mm by 3mm rectangular window. These windows were at the center of a 20mm by 20mm Si die, shown in Figure 2.1. Bulge samples were fabricated from standard semiconductor fabrication methods seen in Figure 2.2.

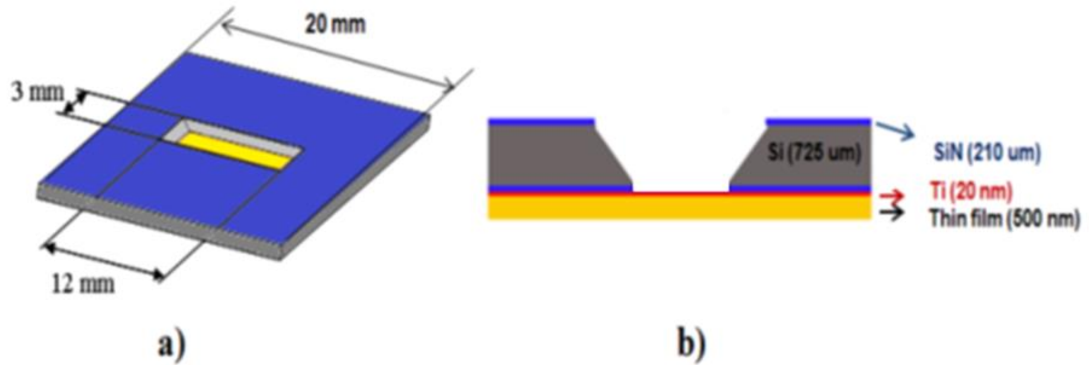

Figure 2.1 a) Bulge sample bottom view, and (b) cross section view.

Silicon dies 725 µm thick were coated on both sides with 210 nm of SiN_x. The back side of SiN_x was patterned by standard photolithography to create a 3mm by 12mm window through etching. The silicon in the window region was etched with 45wt% KOH at 85˚C until only the top SiN_x remained, spanning the window. Acting as an adhesive layer, a 20nm film of Ti was sputtered at 200°C using DC magnetron sputtering on the front side over the SiN_x. Gold thin films were then deposited over the Ti at the same temperature. After metal deposition was completed, the SiN_x window membrane was etched away using reactive ion etching (RIE). This resulted in a freestanding Au/Ti thin film for pressure testing. Deposition and patterning of the SiN_x films was carried out at Bell Laboratories. Etching of silicon and metal deposition were done at Lehigh.

At this point in production, the gold film is under tensile stress after cooling from 200°C due to differences in expansion coefficients between silicon and Au. For bulge test purposes, it is required that the film is perfectly flat when no pressure is applied; i.e. the film must be under tensile stress to prevent buckling and give reliable results [44]. The remaining SiN_x was removed using reactive ion etching with CH_4 gas, leaving behind a

freestanding film of 20nm Ti and 500nm Au. At this point, atomic layer deposition (ALD) was carried out on the samples at different stages of testing the testing process.

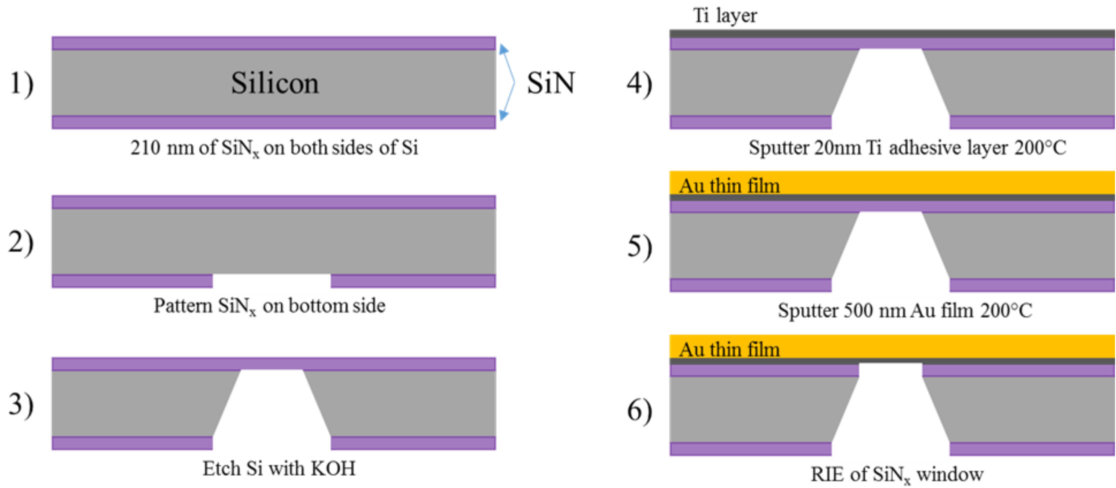

Figure 2.2 Steps of Sample Fabrication for Bulge Testing

2.2 Fabrication of Au films and surface treatments

To limit the effect variation in Au microstructure has on testing to a minimum and analyze only the effect ALD has on viscoelastic/viscoplastic response of the films, all gold sputter parameters were identical for each sputtering event. Each film was sputtered at 200°C at a power of 150W for both Ti and Au. The sputter chamber has multiple targets, making dual sputtering possible. Samples were sputtered at 200°C to provide tensile stress across the film at room temperature and to create a thermally stable microstructure during ALD deposition at 80°C.

Three samples were created and each subjected to a different order of operations with respect to testing and passivation coating. The first of the three was taken from the sputter chamber after venting and allowed to sit in air for 2 weeks before ALD occurred.

After ALD, the sample was bulge tested at room temperature under iso-strain conditions to determine the viscoelastic/viscoplastic response. The second sample was taken from the sputter chamber and immediately subjected to ALD processing. After ALD coating, the sample was subjected to identical bulge testing like sample 1. At this point, any change in behavior between sample 1 and sample 2 will be due to the time at which ALD coating occurred. If there is a change in behavior between the two, it will be attributed to the degree of adsorbed elements that coat the surface during the 2 week sit.

The third sample was taken from the sputter chamber and immediately put in the bulge apparatus for testing. After testing, the sample was subjected to ALD coating before again being bulge tested. For sample 1, it is possible that a 14 day delay between sputtering and coating with ALD could allow enough adsorbed atoms on the film surface to change the interface between Au and ALD as compared to a film that underwent immediate ALD coating. It is also very likely that sample 3 will have accumulated enough adsorbed surface atoms during the initial bulge testing to see similar surface conditions to sample 1. Testing the time dependence of ALD and its effect on steady state behavior between sample 1 and 2 (waiting two weeks before ALD vs. immediate ALD) essentially act as a way of simulating what is happening to the surface of sample 3 without subjecting sample 2 to bulge testing. A schematic of the testing conditions and procedures is shown in Figure 2.3.

To eliminate any additional variables titanium may have on viscoelastic response, two additional samples were created. The first baseline sample followed the exact same steps in Figure 2.2, however, there was no titanium sputtering step. This sample acts as a

baseline for any effect alloying may have on viscoelastic response. The second baseline test follows the same steps in Figure 2.2 but does not undergo RIE of SiN. This sample will determine any effect SiN may have on viscoelasticity.

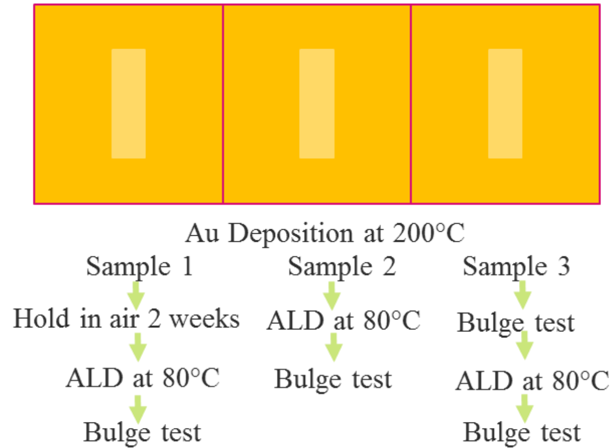

Figure 2.3 Au films under identical sputtering conditions with testing procedures

2.3 Bulge testing

2.3.1 Bulge measurement technique

Bulging of the membrane can be controlled by manipulating the change in gas pressure across the film. This difference in pressure is established by first maintaining vacuum on both sides of the membrane before introducing argon pressure on the back side of the film. The argon pressure is controlled via an MKS pressure controller set up with a LabView program. The overall height change of the film is determined via changes in capacitor signals. In this experiment, the bulging film itself is treated as one of the plates of a capacitor (Figure 2.4) and changes of the bulge capacitance are recorded as a function of applied pressure to the film. In the figure, B is the gap spacing between

plates, D is the membrane width, H is the height of the bulged film, R is the induced radius of curvature created by the bulge, and b is the length of the membrane.

The setup consists of a fixed capacitor plate 6 mm by 6 mm surrounded by a closely spaced guard ring set to ground in order to limit the fringing field. This plate is positioned over the center of the 3mm by 12mm membrane specimen set 165 μm away. The size of the plate opposite the membrane is wide enough so that the capacitance is insensitive to exact specimen placement. It is also short enough to measure only the central 6mm of the bulge, avoiding both ends with the more complicated shape. Vlassak and Nix [30] have found that for a rectangular membrane with an aspect ratio greater than 4, the deflection at the center of the membrane can be approximated with the exact solution for an infinitely long rectangular membrane. This setup takes advantage of this approximation and only measures height changes of the mathematically simpler region.

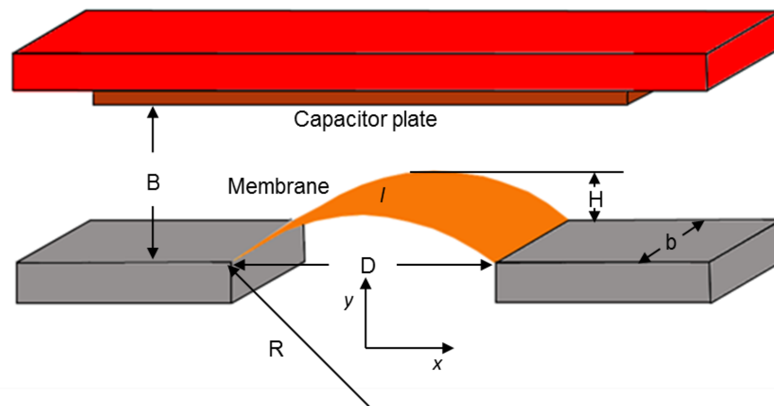

Figure 2.4 Method of bulge test with known geometrical parameters

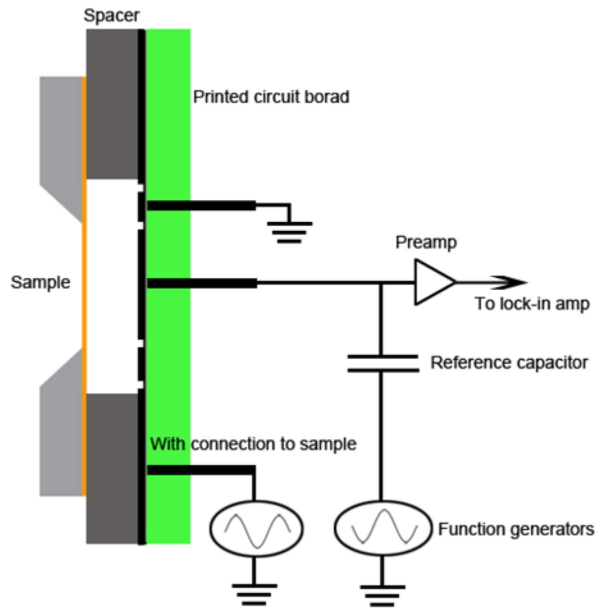

Figure 2.5 Electrical setup of bulge test

Figure 2.5 depicts the electrical circuit setup for capacitance measurements. In order to directly measure the capacitance, function generators apply a sine wave of 100 kHz to the bulge capacitor and a reference capacitor with known capacitance. The two sine waves are phase locked and shifted 180˚ to make them completely out of phase with one another. The phase currents from each capacitor are summed in a charge sensitive preamplifier which sends the output to a lock-in amplifier whose reference signal is from one of the function generators. Changing the amplitude of one of the 100 kHz signals allows the current flowing through the two capacitors to be equal. This will show a lock-in signal of zero. At this point of balance, the ratio of the two capacitances is inversely proportional to the ratio of amplitudes of peak-to-peak voltage of the two sine waves. To develop a linear relationship of lock-in output vs. current difference curve, the AC

voltage applied to the bulge capacitor is arbitrarily offset by a small amount. This offset creates a directly proportional change of lock-in signal and bulge capacitance while avoiding the sum of voltage reaching 0. The relationship between bulge capacitor and reference capacitor can be seen below:

$$\boldsymbol{L = k(V_0 C_0 - V_1 C_1)} \tag{2.1}$$

where L is the lock-in signal, k is a lock in constant calibrated for the lock in amplifier, V_0 is the applied voltage to the bulge capacitor, C_0 is the capacitance value of the bulge, V_1 is the applied voltage to the reference capacitor and C_1 is the capacitance of the reference capacitor. As the thin film is bulged due to an increase in pressure, any change in the lock-in signal will be due only to the bulged membrane. Any change in lock in signal can be translated to a change in bulge capacitance of the membrane.

Because the system is based on capacitance measurement, by measuring capacitance, C, between the membrane and the fixed electrode, the radius of the film can be calculated:

$$C = 4\varepsilon_0 b \frac{\sqrt{4R^2 - D^2} \cdot \arctan\left(\dfrac{D}{\sqrt{4B\sqrt{4R^2 - D^2} - D^2}}\right)}{\sqrt{4B\sqrt{4R^2 - D^2} - D^2}} \tag{2.2}$$

where ε_0 is the permittivity of free space (8.854 X 10^{-12} F/m), b is the effective width of the capacitor plate on the fixed electrode (6.17 mm; to account for fringing fields, 0.17 mm must be added), and D is the width of the membrane (3 mm).

The bulged membrane in the center region can be treated as a cylindrical surface with radius, R (Figure 2.4). This allows the stress to be approximated as:

$$\sigma = \frac{p \cdot R}{t} \tag{2.3}$$

where p is the gas pressure and t is the membrane thickness. Strain of the membrane is defined by:

$$\varepsilon = \frac{l - D}{D} = \frac{2R \cdot \arcsin\left(\frac{D}{2R}\right) - D}{D} \tag{2.4}$$

where D is the width of the membrane in Figure 2.4.

Because of the complexity of Equation 2.2 in deriving R followed by H, it is much simpler and computationally time effective to create a 4 term polynomial function relating delta C to bulge height. By adjusting the input parameters for membrane geometry, the delta C vs H plot can easily be created to quickly convert the capacitance values output from Labview into stress and strain. An example of a fitting function used is given in Figure 2.6.

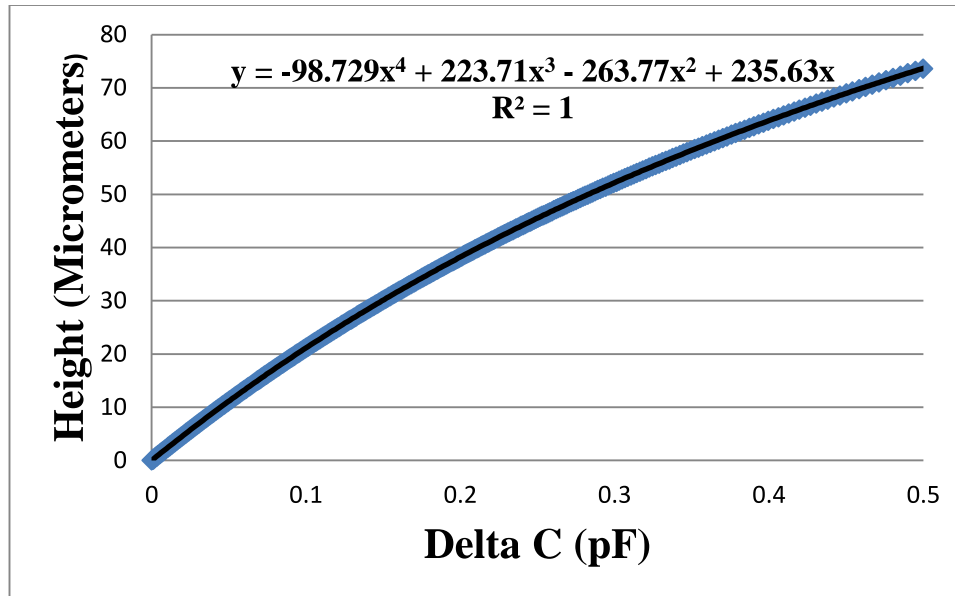

Figure 2.6 Example of 4 term polynomial fit function to describe the relationship between C and bulge height.

Thickness of metal layers and ALD thickness were determined via EPMA and the Pouchou Pichoir Method [45]. Film thickness is determined via the k-ratio of signal for a given element in the film compared the signal of the pure element. A phi-rho-z fit was also used during analysis. Using silicon as a substrate, SiKα photons did not have enough energy to penetrate Au or Ti thin films, which simplified phi-rho-z relationships. It was experimentally determined that ALD thickness was 7.5nm, Au thickness was 500nm, and Ti thickness was 17nm.

Surface passivation thickness required a deposition process that created a stoichiometric coating. It has been proven [46] that for Al_2O_3 films deposited using trimethylaluminum (TMA) and H_2O at deposition temperatures as low as 58°C created an element ratio of O/Al of 1.5. For this reason, ALD was conducted using TMA and H_2O at

a temperature of 80°C. Because Au and Ti were sputtered at 200°C, the metal films should be microstructurally stable at 80°C during ALD.

2.3.2 Stress relaxation experiments

Viscoelastic behavior of Au films was examined by keeping films at a fixed applied strain of approximately 0.1%. Pressure required to reach 0.1% strain was determined via a pressure ramp similar to Figure 2.7. From these pressure ramps, both the biaxial modulus and the residual stress can be determined. Each sample was tested at different pressure loading/unloading rates to determine the change in biaxial modulus with rate. For all tests, the biaxial modulus was taken from data between 0.08% and 0.1% strain on the unloading portion of the curve to further reduce the effect that the pressure ramp may have on biaxial modulus measurements.

Because of the plane strain loading conditions applied to the film, all modulus numbers taken during testing are referred to as the plane strain modulus. Converting to uniaxial modulus, E, requires use of Poisson's ratio:

$$\boldsymbol{E = E_{PS}(1 - v^2)} \tag{2.5}$$

where E_{PS} is the plane strain modulus and v is Poisson's ratio (0.42 for Au). A plane strain modulus of 95.9GPa translates to a uniaxial modulus of 79GPa. In this study, all drops in modulus with time during iso-strain tests are normalized to the initial modulus from the pressure ramps. Stress relaxation experiments were run for 3 hours each.

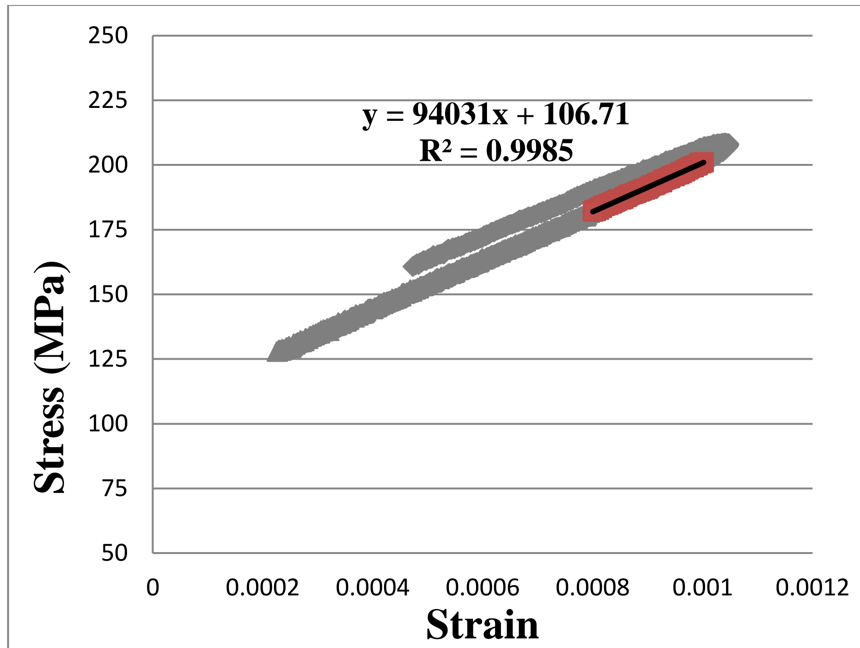

Figure 2.7 Typical pressure ramp to determine plane strain modulus and residual stress in films

For consistency, all runs for every sample had to be switched from pressure ramps to iso-strain holds in the same manner in order to keep start times of stress relaxation recordings constant. Switching from ramp mode (mode 1) to iso-strain mode (mode 2) requires the film to be in a stable condition where the film capacitance has stabilized (pressure applied to the film is constant). Empirical results show that waiting 5 seconds after the ramp has reached the desired pressure on the up-swing (there is slight overshoot in pressure before equilibration at desired pressure) before switching to mode 2 creates the smoothest transition in the software. Iso-strain start times for modulus recordings therefore start 5 seconds after the initial pressure has been reached.

3. Results and Discussion

3.1 Iso-strain conditions for pure gold

As a baseline for experiments, a pure 500nm gold sputtered film was created in order to determine any effects a passivation layer or a titanium adhesive layer may have on initial and steady state anelastic behavior (Figure 3.1). The normalized effective modulus was calculated for all tests as the plane strain modulus at a given time M(t), divided by the initial modulus M(t=0). The normalized effective modulus is calculated using:

$$M(t) = \frac{\sigma(t) - \sigma_0}{\varepsilon(t)} \tag{3.1}$$

where σ(t) is the stress in the film at a given time, σ_0 is the residual stress in the film calculated from a pressure ramp, and ε(t) is the strain at any given time (constant in iso-strain conditions as 0.1%) The first run normalized modulus initially decreased to 0.756. This indicates a drop in modulus to just 75.6% of the initial modulus.

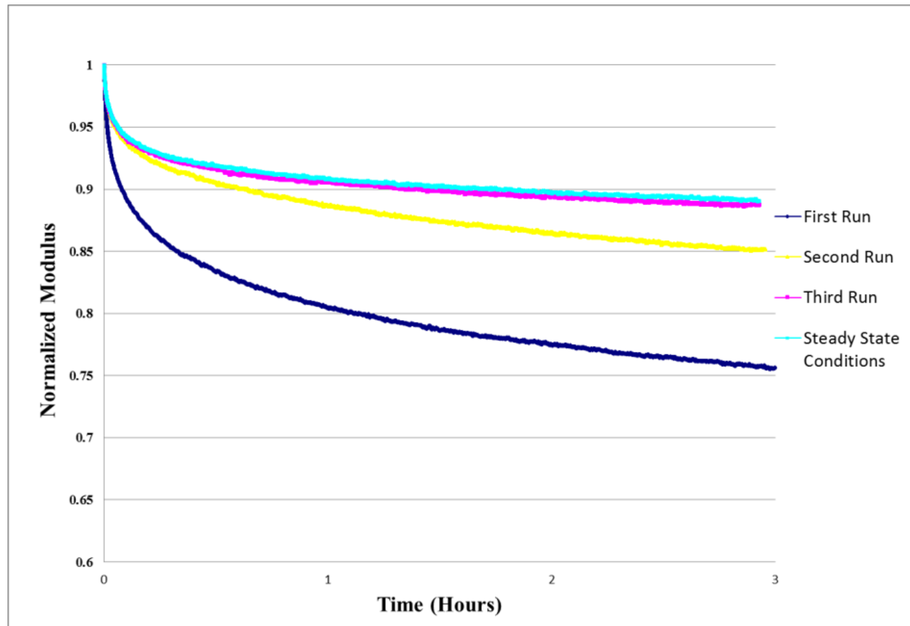

Figure 3.1 Normalized modulus iso-strain curves for pure freestanding gold

An additional 3 runs were conducted at 0.1% strain after the first run was completed to determine steady state behavior. In order to determine the pressure required to reach the prescribed strain of 0.1%, pressure ramps were conducted at least 18 hours after each iso-strain run completion in order to allow enough time for total recovery in the film. These ramps would provide not only the required pressure, but would also identify any changes in modulus or residual stress. A plot of plane strain modulus and film residual stress for each run is shown in Figure 3.2.

Plane strain modulus values for gold (and all subsequent tests) are all relatively constant at about 93 GPa, which translates to a uniaxial modulus of 76.6 GPa. This value corresponds well to literature values of 78 GPa. The degree of change in residual stress in the film with respect to run number can qualitatively correspond to the degree of viscoplasticity acting in the film. Before testing, when the viscoplastic behavior has not

yet been exercised, the residual stress is highest at 59.2 MPa. After run 1 is completed the residual stress drops 18.5% to 48.2MPa. After this first initial drop, the residual stress levels off to roughly 46.6MPa. The decrease in viscoplastic response of the film displays similar behavior to that of residual stress. The large drop in viscoplasticity between run 1 and run 2 suggests that stabilizing the residual stress in the film through each run cycle may have an effect on the viscoplastic behavior of the film.

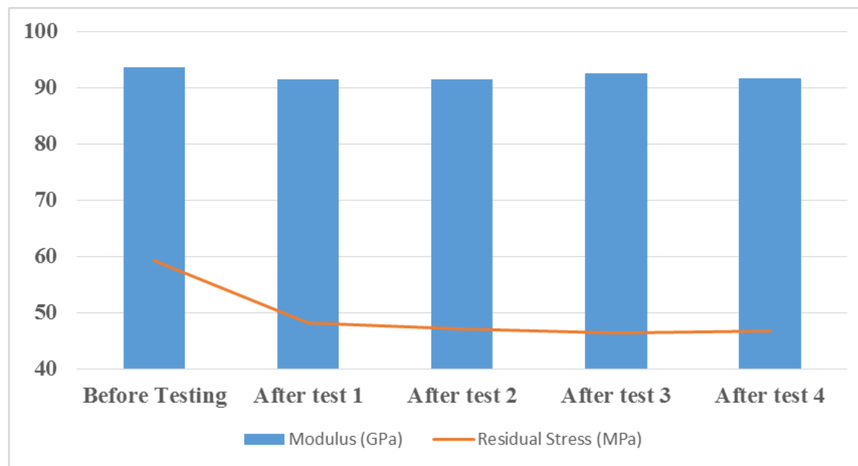

Figure 3.2 Modulus and residual stress changes in pure Au film throughout testing cycles

3.2 Iso-strain conditions for uncoated sample

Anelastic behavior of 500nm of gold deposited on 20nm of adhesive Ti was also analyzed. It is apparent that the initial relaxation curve follows a similar path as the pure Au case, however the Au/Ti film had a slightly larger normalized modulus reduction compared to pure Au; 35.4% and 24.4% reduction respectively (Figure 3.3). However, steady state behavior between the two is close at 11% for the pure Au and 13.3% reduction for the Au/Ti film. This suggests that the presence of titanium as an adhesive layer does very little to change the steady state behavior at this testing temperature

despite the differences in grain size. Previous tests of pure gold films under the same processing conditions displayed a grain diameter of 460nm [36]. The Au/Ti films from this work had a resulting grain size of 174nm. However, at room temperature, despite the increase in grain boundary volume for Au/Ti, samples behaved in a very similar manner to the pure Au film, suggesting that grain boundary diffusion is not a significant contributor to viscoelasticity at this temperature.

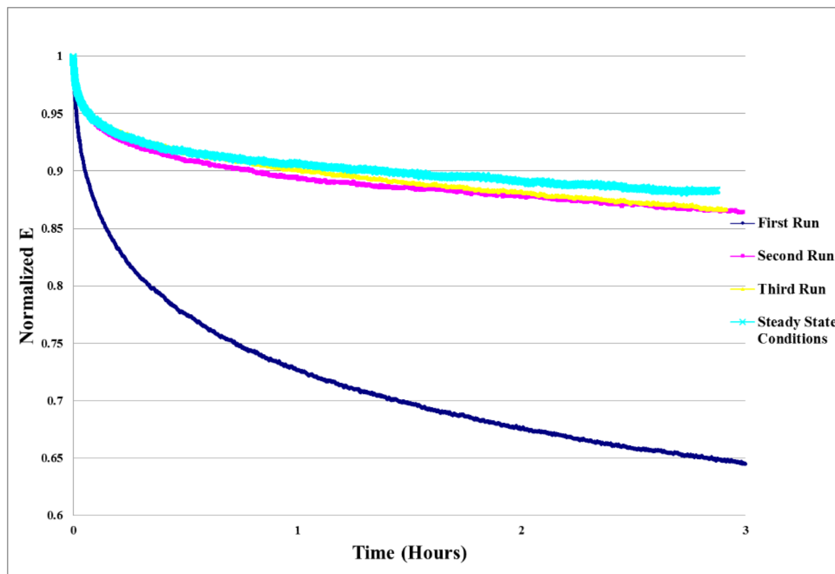

Figure 3.3 Normalized modulus iso-strain curves for freestanding uncoated Au on Titanium

Residual stress in the uncoated Au/Ti film is much higher than the pure Au film. This could be due to a lower substrate induced residual stress in the film caused by a lower adhesive strength between Au and SiN_x than Ti and SiN_x. However, with respect to viscoplasticity and drop in residual stress, the same trend seen in the pure gold film is apparent in the Au/Ti film. There is statistically no difference in residual stress values between subsequent tests after test 1 has completed. Also, the relatively large change in

viscoplastic behavior between run 1 and run 2 is also very apparent in figure 3.3. After run 2, there is only slight changes in anelastic response compared to steady state behavior.

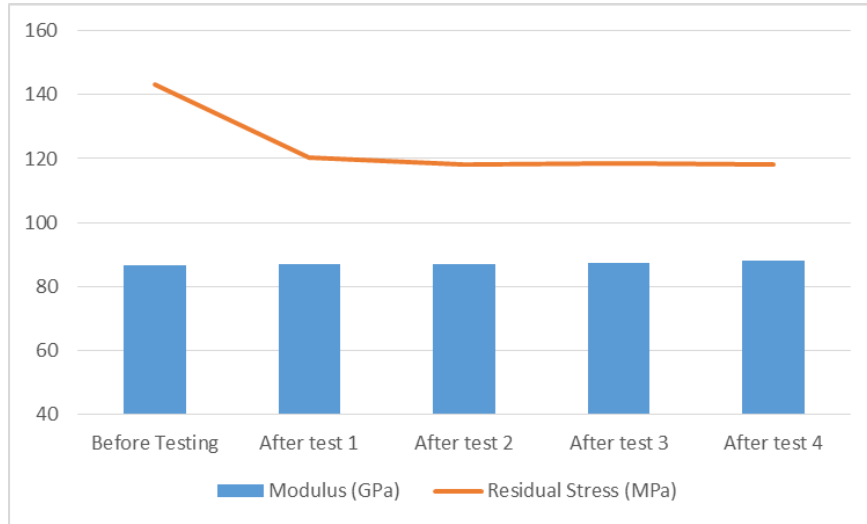

Figure 3.4 Modulus and residual stress changes in uncoated Au on Ti film throughout testing cycles

3.3 Iso-strain conditions for ALD coated samples

Three separate ALD samples were prepared in order to determine whether steady state behavior is susceptible to a passivation layer, and if so, is there any time dependence for when the passivation layer was created relative to sample creation. In addition, any changes a passivation layer may have on an uncoated sample already at steady state were also analyzed.

In Figure 3.5, the normalized time dependent plane strain modulus reduction for each subsequent iso-strain run is shown for the sample immediately subjected to surface passivation. In this scenario, after sputter deposition and RIE etching of SiN_x, the sample was quickly subjected to ALD surface treatment. It is apparent that even with the

presence of a passivation layer, the initial relaxation behavior is comparable to uncoated samples. With an initial modulus reduction of 27.3%, it is within the range of the pure Au and uncoated Au/Ti sample. The steady state condition is statistically indistinguishable from steady state conditions in the pure Au and uncoated Au/Ti samples. A compilation of initial modulus reduction and steady state modulus reduction can be seen in Table 3.1 for pure gold, gold on titanium, and for various Al_2O_3 treatments.

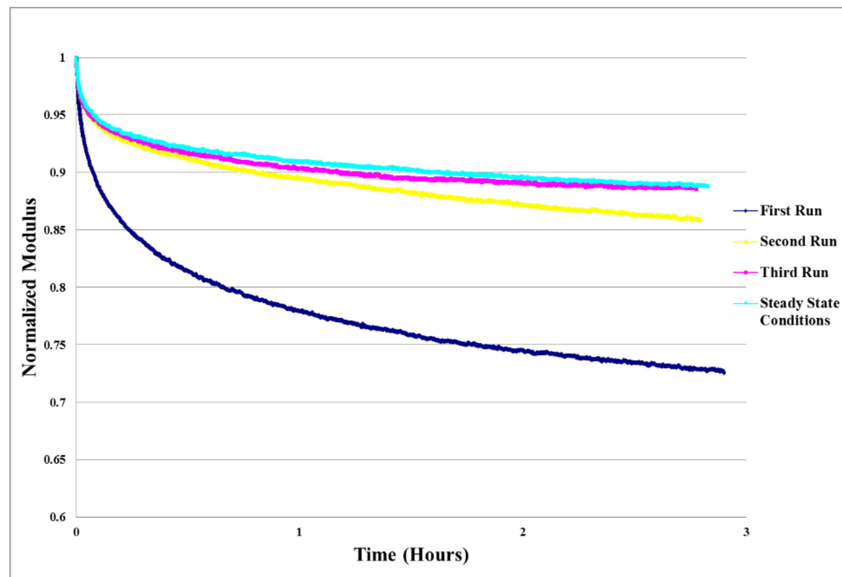

Figure 3.5 Normalized modulus iso-strain curves for freestanding Au on Ti coated with passivation layer immediately after film sputtering

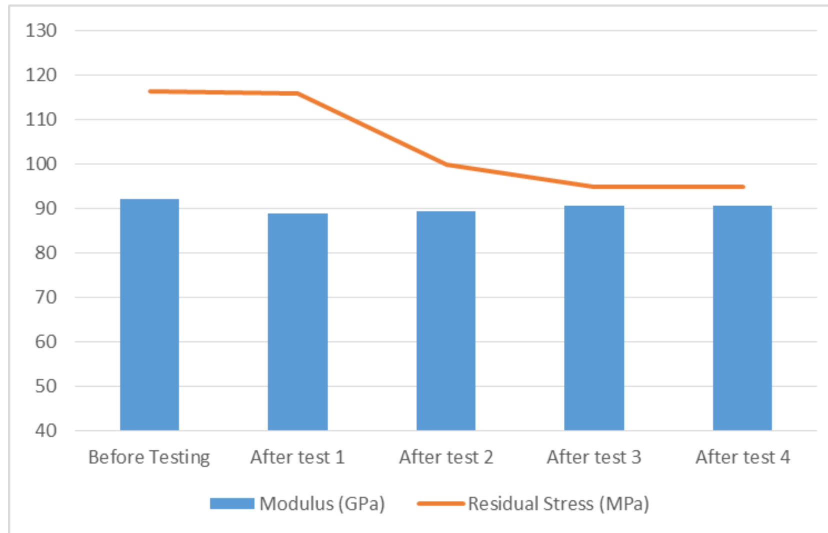

Figure 3.6 Modulus and residual stress changes throughout testing cycles of Au on Ti films subjected to passivation immediately after sputtering

Figure 3.7 shows the normalized time dependent plane strain modulus reduction for each iso-strain run for a sample which was delayed 2 weeks after sputtering before subjected to ALD coating. Figure 3.8 shows the same behavior for a sample subjected to surface passivation deposition after the uncoated sample had reached steady state behavior. Note, the second run in Figure 3.8 exhibited signal drift in the function generators creating an artifact that appears to make the reduced modulus increase in time. This run was ignored.

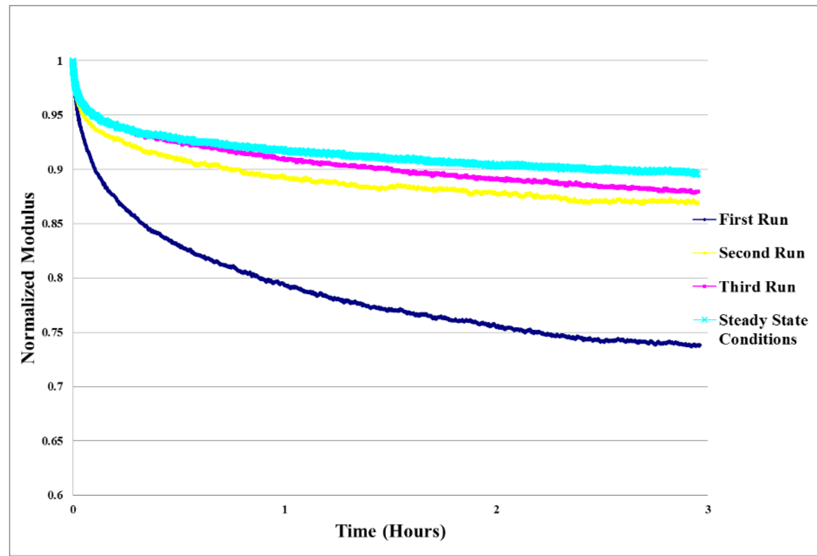

Figure 3.7 Normalized modulus of iso-strain curves for coated Au on Ti. Passivation layer was deposited 2 weeks after initial sputtering.

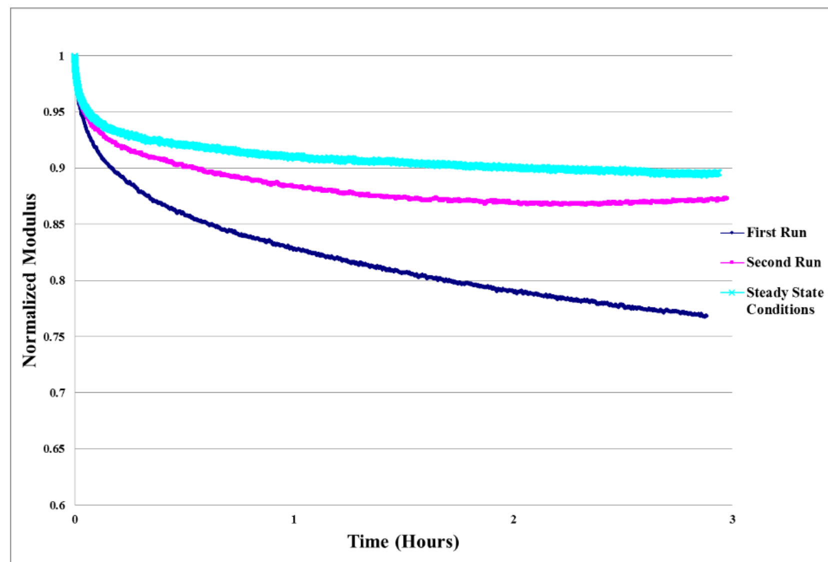

Figure 3.8 Normalized modulus of iso-strain curves for ALD coated Au on Ti. Passivation layer was deposited after uncoated sample had reached steady state conditions

Figure 3.9-3.11 show the change in residual stress for each run for the three ALD coated samples. The same trends seen above for the uncoated samples is apparent in the

ALD coated samples. It appears that 7.5nm passivation layer thickness is insufficient in preventing stress relaxation throughout test cycles in the films at this temperature.

		Modulus % Reduction
Pure Au	**Initial**	**24.4**
	Steady State	*11*
No ALD	**Initial**	**35.4**
	Steady State	*13.3*
Immediate ALD	**Initial**	**27.3**
	Steady State	*11.1*
14 day sit then ALD	**Initial**	**25.9**
	Steady State	*10*
ALD after steady state of uncoated sample	**Initial**	**22.7**
	Steady State	*10.6*

Table 3.1 Compilations of initial and steady state behavior of samples tested

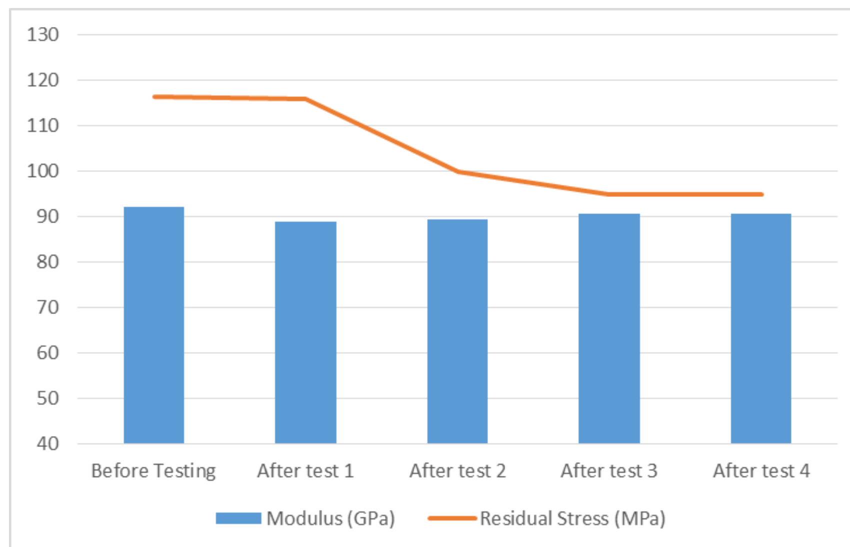

Figure 3.9 Modulus and residual stress changes throughout testing cycles of Au on Ti films subjected to passivation immediately after sputtering

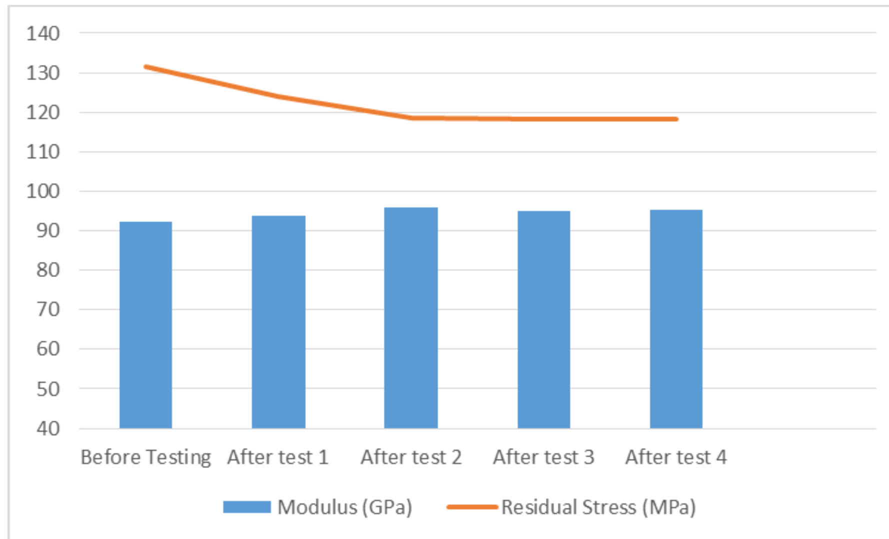

Figure 3.10 Modulus and residual stress changes throughout testing cycles of Au on Ti films subjected to passivation 2 weeks after sputtering

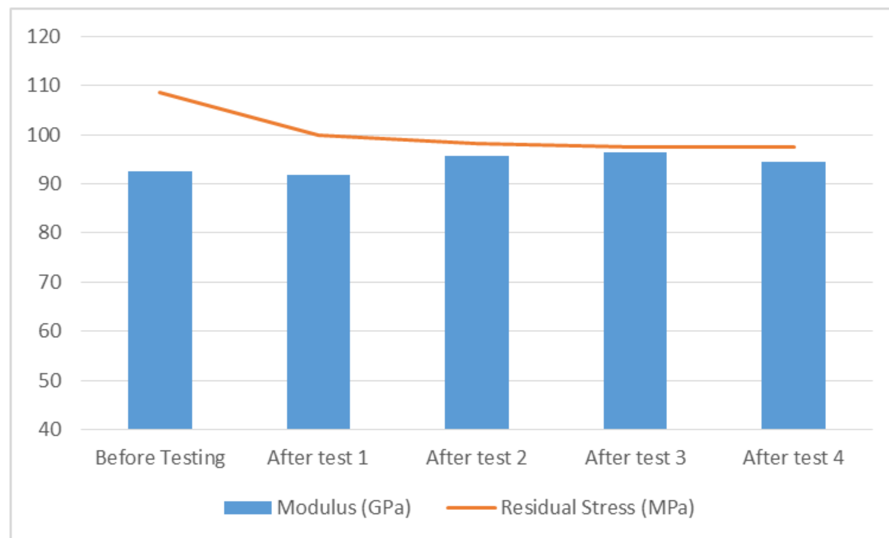

Figure 3.11 Modulus and residual stress changes throughout testing cycles of Au on Ti films subjected to passivation after uncoated sample reached steady state conditions

Figure 3.12 and 3.13 show the effect iso-strain cycles have on plane strain modulus and residual stress, respectively. It can be seen that after recovery, each

sample's modulus returns to the original value. However, residual stress in the film has a noticeable change with respect to number of iso-strain runs.

Initial and steady state comparisons of tests are shown in Figure 3.12 and 3.13, respectively. Sufficient variability in the data and lack of statistical reliability prevents conclusive differentiation between initial and steady state stress relaxation behaviors between samples. It can be concluded that at these temperatures the effect an ALD coating has on steady state behavior seems to be nonexistent. The pure Au film behaved identically to Au/Ti films with/without ALD, suggesting that the Ti adhesive layer does not contribute to any behavior change at this temperature.

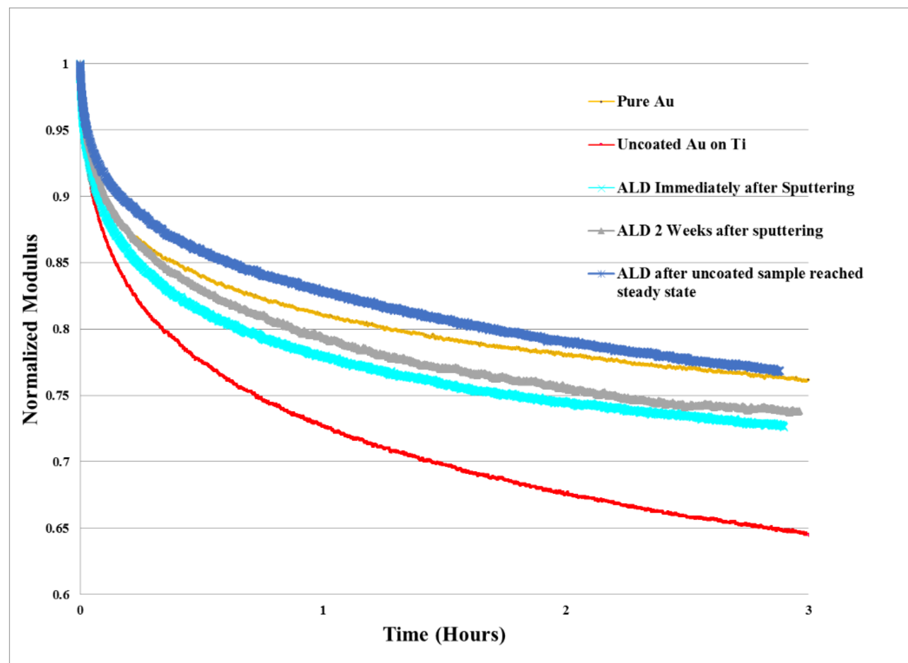

Figure 3.12 Initial stress relaxation behavior of tests

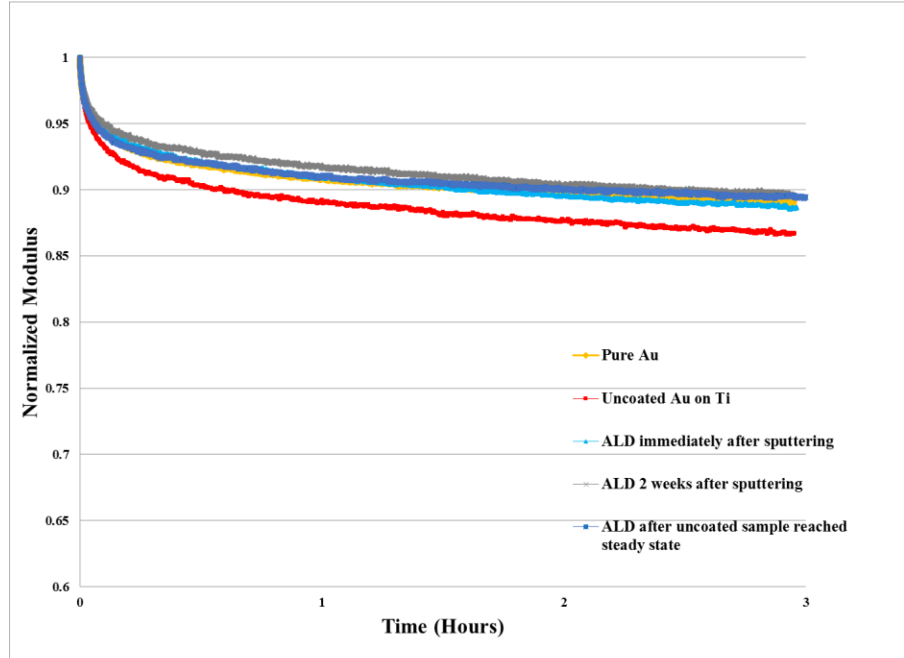

Figure 3.13 Steady state behavior of all tests

3.4 Iso-strain conditions for film on SiN_x substrate

To determine if the SiN_x had any effect on initial or steady state behavior, an additional sample under identical fabrication procedures was tested. The presence of SiN_x can be excluded from analysis via the equation for composite modulus:

$$M_{composite} = \frac{M_{Au}t_{Au} + M_{SiN}t_{SiN}}{t_{Au} + t_{SiN}} \quad (3.2)$$

where M_{Au} is the experimentally determine plane strain modulus of gold, t_{Au} is the gold film thickness, M_{SiN} is the plane strain modulus of SiN_x, and t_{SiN} is the thickness of SiN_x. In order to empirically determine the plane strain modulus of SiN_x, the modulus of pure Au films was used through equation 3.2. This produced a silicon nitride modulus of 160GPa. This number is much lower than literature values, due to the likelihood that SiN_x may have been partially etched during the KOH etch of silicon. SiNx, has been shows to

etch at about 1nm/hour under the 45%KOH at 85°C [47]. This would create a thinner film of silicon nitride and create a lower modulus under the assumption that the film stayed 210 nm thick. The exact modulus value for SiN_x in this experiment was not significant because its contribution to Au relaxation behavior was removed from analysis. Figure 3.14 displayed the anelastic behavior of gold film on a SiN_x substrate. It can be seen that the overall behavior follows a similar trend to samples not tested with SiN_x.

Initial drop in normalized plane strain modulus for Au/Ti thin films on silicon nitride was very similar to previous test behavior. For the first run, the modulus dropped 23.3% from initial modulus value. Steady state behavior displayed a drop in normalized modulus of 10.9%. It can be concluded that at these testing temperatures there is no statistical change in film behavior with or without the presence of a SiN_x substrate for either initial or steady state behavior.

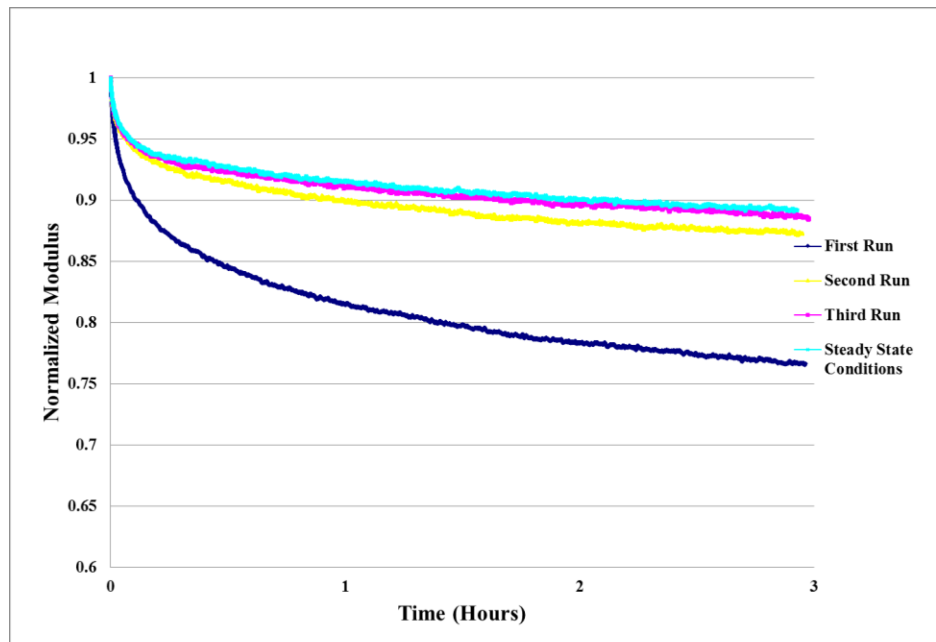

Figure 3.14 Normalized modulus of iso-strain curves for coated Au/Ti on SiN_x.

3.5 Iso-Strain Conditions with 20nm TiO_2

A final test was conducted to determine the effect surface oxide thickness may have on anelastic behavior. Due to a depleted source of TMA for Al_2O_3 ALD, the precursor was switched to TDMAT and deposited at 80°C. Instead of 7.5nm Al_20_3 passivation layer on previous tests, this test had 20nm thick layer of TiO_2. For these experiments, the actual composition of the passivation layer was less important than its presence and any resulting effect on film behavior. Previous tests with Al_20_3 had a total thickness of 15nm (7.5nm on the top surface and 7.5nm on the bottom surface). The effect 15nm of Al_2O_3 has on the gold film modulus was ignored due to the total thickness being much larger and the fact that amorphous Al_20_3 has a bulk modulus very similar to gold at 70GPa [48].

Unlike Al_2O_3, the contribution of an additional 40nm of TiO_2 cannot be ignored. Because the modulus of amorphous TiO2 has been shown to range between 140-170 GPa [48], its effect on composite modulus was also removed from analysis the same way the SiNx substrate was removed from analysis by Eq. 3.2. For better comparison, all tests conducted only analyze the behavior of gold (and sometimes Au/Ti) rather than a composite modulus.

Figure 3.15 shows the normalized modulus of iso-strain curves for Au/Ti films coated with 20nm on each side with TiO_2. The same behavior in previous tests can also be seen for the sample with a much larger passivated thickness. Initially the normalized modulus drops to 74.2 - or a drop of 25.8%. At steady state, the viscoelastic response

shows a modulus drop of 12.3%. Figures 3.16 and 3.17 show combined plots of all tests for initial behavior and steady state behavior, respectively.

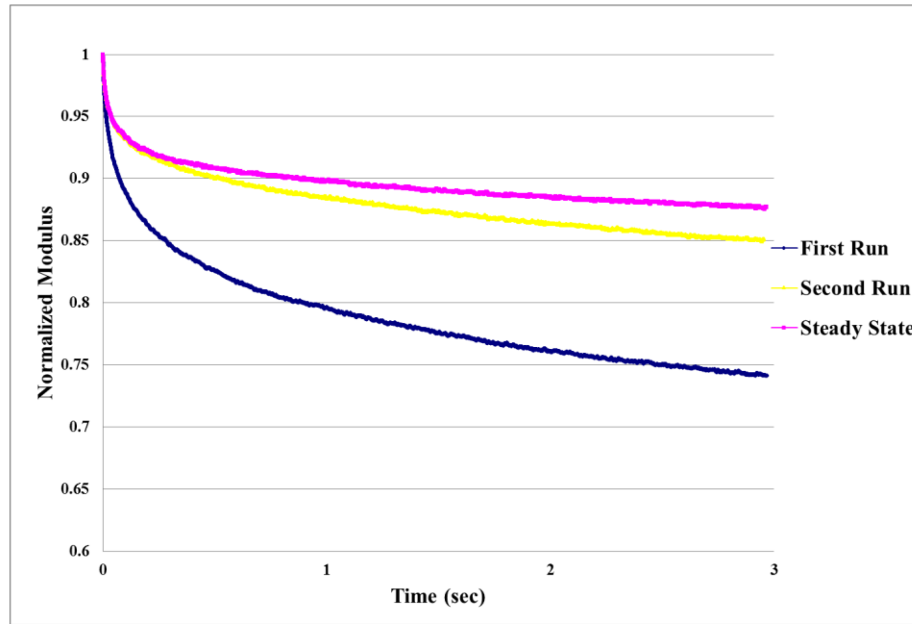

Figure 3.15 Normalized modulus of iso-strain curves for 20nm of TiO_2 on Au/Ti film

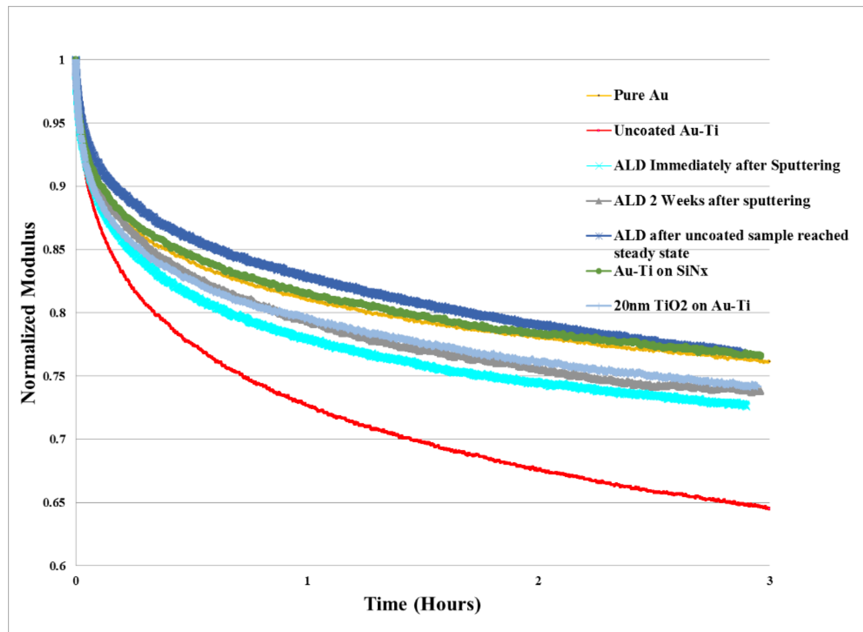

Figure 3.16 Initial stress relaxation behavior for tested samples

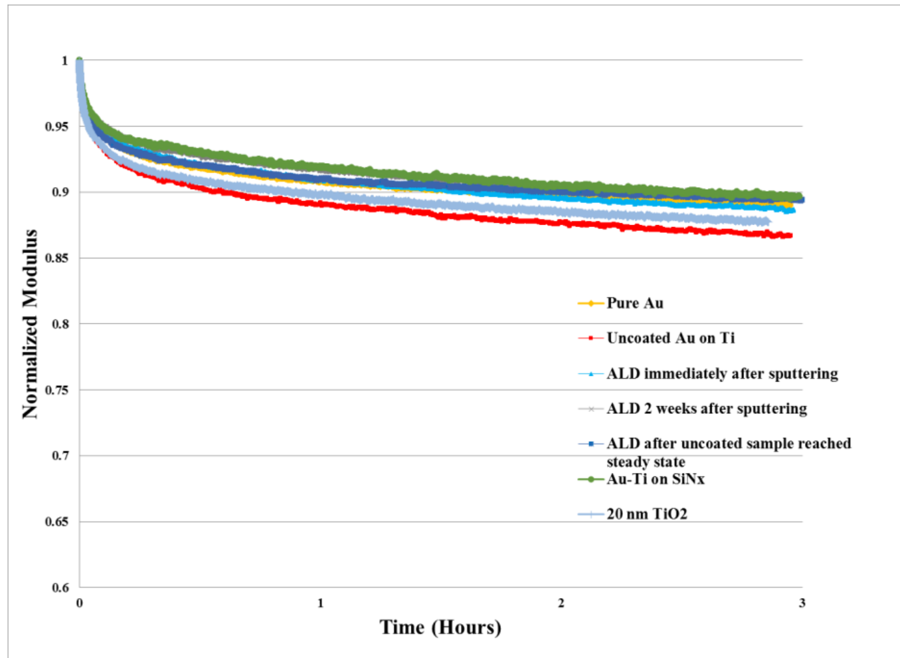

Figure 3.17 Steady state behavior for all tested sample

It can be seen from figure 3.17 and table 3.2 that surface passivation layer type, thickness, and deposition time with respect to film exposure to atmosphere have no statistical effect on steady state behavior of Au/Ti thin films. It also can be concluded that a titanium adhesive layer does not change the steady state behavior; even though Au/Ti films have a smaller grain size (174nm) compared to pure Au (460nm).

		Modulus % Reduction
Pure Au	**Initial**	**24.4**
	Steady State	*11*
No ALD	**Initial**	**35.4**
	Steady State	*13.3*
Immediate ALD	**Initial**	**27.3**
	Steady State	*11.1*
14 day sit then ALD	**Initial**	**25.9**
	Steady State	*10*
ALD after steady state of uncoated sample	**Initial**	**22.7**
	Steady State	*10.6*
Au-Ti on SiN_x	**Initial**	**23.4**
	Steady State	*10.3*
20nm TiO_2	**Initial**	**25.8**
	Steady State	*12.3*

Table 3.2 Compilation of initial and steady state % drops in biaxial modulus of films

3.6 Theories for comparable iso-strain behavior of tests

3.6.1. Ti Passivation Layer

There are several possible reasons why initial and steady state behavior of conducted tests behave in such a similar manner. The first theory is that during 200°C sputtering of films, Ti may have sufficient diffusivity in gold (most likely through grain boundaries) to have enough presence on the surface of the film after 500nm of Au is sputtered. It has been determined that the diffusion coefficient of Ti in Au at 200°C is 5.7×10^{-18} cm^2/s [49]. At this temperature, there may be sufficient driving force for diffusion during Au sputtering to slightly coat the final surface of Au with a thin layer of Ti. If this occurs, the surface Ti will oxidize when exposed to ambient environment and become a passivation layer. The intrinsic passivation layer will then cause any additional ALD coatings to be redundant. The intrinsic TiO2 layer would then be the primary cause

of stopping diffusion and dislocation annihilation. A schematic of this theory is presented in Figure 3.18.

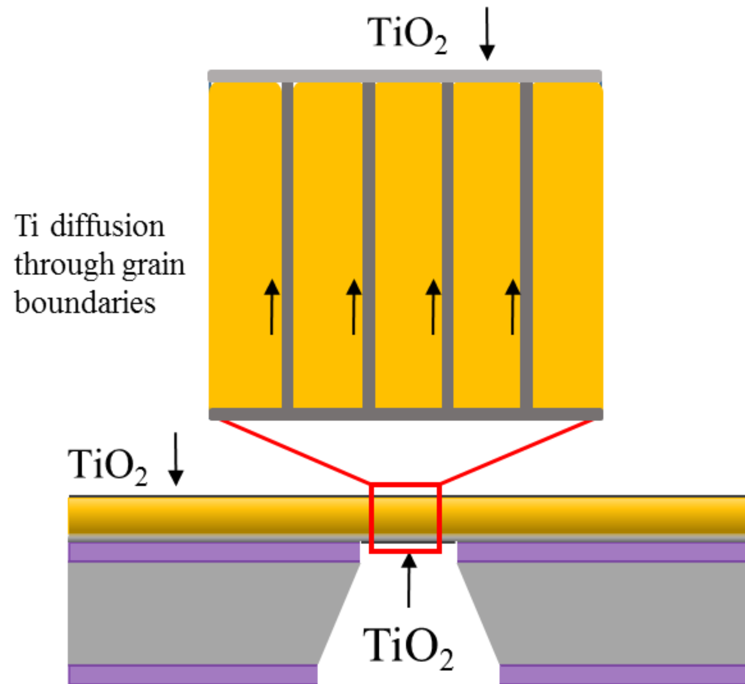

Figure 3.18 Schematic portraying titanium diffusion to the surface via the grain boundaries.

To test this theory, and determine if there is any titanium on the surface of uncoated films, Low Energy Ion Spectroscopy (LEIS) was conducted on an uncoated Au/Ti sample. Primary ion beam consisted of 3 keV He+ with a dose of $2x10^{14}$ ions/cm^2. Sputter cleaning of the sample was done with 0.5kV Ar^+ at a dose of $1x10^{15}/cm^2$ – corresponding to about 1 monolayer of removed material per dose. Three separate scans were conducted. The first scan was done without ion cleaning of the surface, allowing detection of adsorbed atoms. The second scan was conducted after 1 dose of cleaning to remove 1 monolayer. The third scan was conducted in a different region with 2 doses of

cleaning to remove 2 monolayers. The recorded peaks for each scan can be seen in figure 3.19.

Without cleaning the surface, contaminant elements from ambient environment (C, O, K) are labeled. There is a very small peak where Au should be, however it is reduced significantly due to the presence of contaminants. There is no evidence of a titanium peak under these circumstances.

Subjecting the surface to one dose of cleaning (one monolayer removal), there is appears to be no evidence of titanium. A second dose of cleaning proves that there is no titanium at the surface and the entirety of surface atoms are gold atoms.

A depth profile was then taken in another region of the film in attempt to discern a potential change in Ti concentration near the surface. Figure 3.20 shows the depth profile of Au signal and an integral signal taken from the low energy part of the spectra. The Au signal appears to reach a plateau in signal strength. The low energy integral signal is indicative of the level of surface contamination, which also plateaus at the same depth as the Au plateau. It can be concluded that this techniques sensitivity limit (approx. 0.1 atomic%) cannot detect any Ti for the first several monolayers of material. This technique adequately disproves the possibility of titanium diffusion to the surface of the gold.

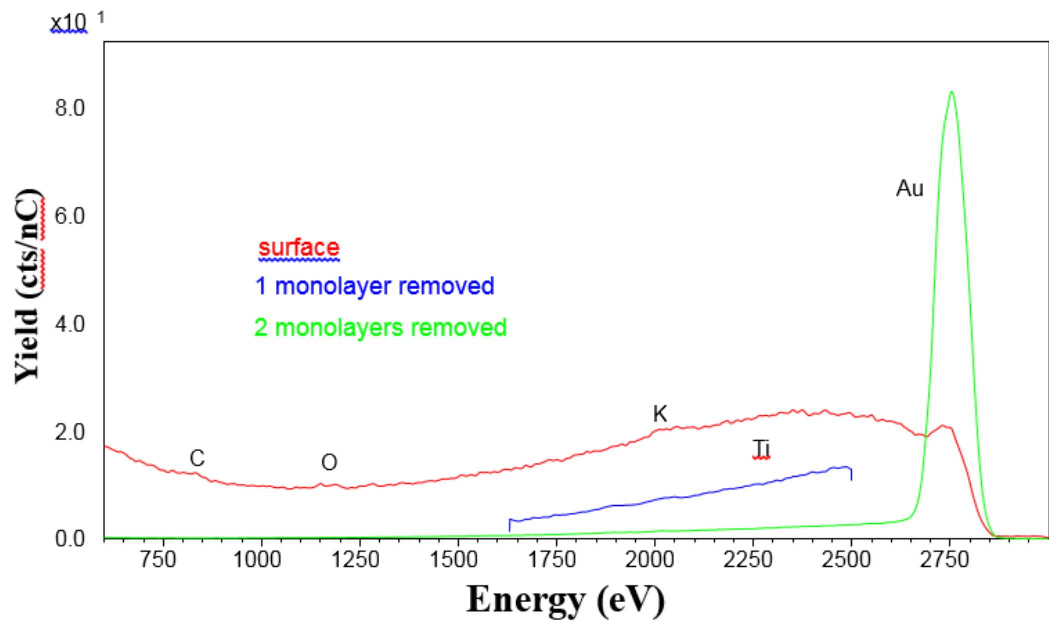

Figure 3.19Au/Ti film LEIS analysis showing presence of atoms on the surface, one monolayer deep, and 2 monolayers deep

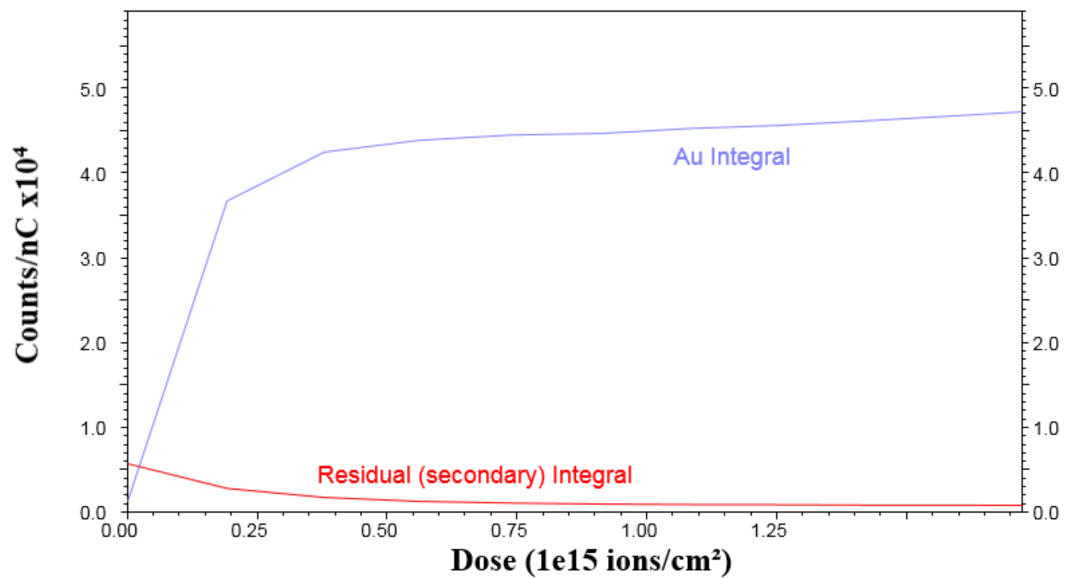

Figure 3.20 Depth profile showing a plateau of gold signal with depth

3.6.2. Grain Boundary Sliding

Another mechanism that has been known to induce anelastic response in films is grain boundary sliding/diffusion [50]. Wei et. al. examined partially recoverable creep deformation from heterogeneous grain boundary sliding of 50nm films in FCC metals at temperature between 300-500K. They argue that theoretical modeling, experiments, MD, simulations, and discrete dislocation simulations suggest GB diffusion plays an important or dominant role in unpassivated Cu films thinner than 200nm. They also observed a transition from diffusion/sliding-dominated deformation in 50nm thick films to a dislocation dominated deformation behavior in 200nm thick films. For current films of 500nm thicknesses, it is likely the deformation mechanism is not grain boundary diffusion/sliding, but dislocation based.

3.6.3. Dislocation Based Mechanism

Additional mathematical approximations can be made to support the dislocation motion theory over other mechanisms being responsible for steady state viscoelastic behavior of thin films. A steady state normalized modulus curve can be described as a purely viscoelastic response of a time dependent reduction in film stress, $\Delta\sigma$. This reduction can be attributed to the strain change caused by viscoelasticity, $\varepsilon_{Viscoelastic}$.

For a change of stress of 11% (comparable to what we have seen for steady state behavior, seen in Figure 3.21), the change in strain due to viscoelastic response is approximately 1.17×10^{-4}. Given the lattice spacing of gold to be 0.408nm, the magnitude of Burger's vector for the gold system is |b|=0.228nm. Assuming the mean free path of a

dislocation to be 87nm (half the grain size) gives a dislocation density to be $4.67 \times 10^{12}/m^2$:

$$\varepsilon_{Viscoelastic} = b\rho_m\bar{x} \tag{3.3}$$

where b is the Burgers vector, ρ_m is the density of mobile dislocations, and $\bar{\boldsymbol{x}}$ is the mean free path of a dislocation. This density corresponds to an average dislocation length per grain of 70.7nm. This is much smaller than the average grain diameter of 174nm, suggesting that random grains have the capability of holding several of these dislocations. If we assume the length of a dislocation can only be a tenth of the grain diameter, a total dislocation motion of 70.7nm can still be accommodated by just 4 dislocations.

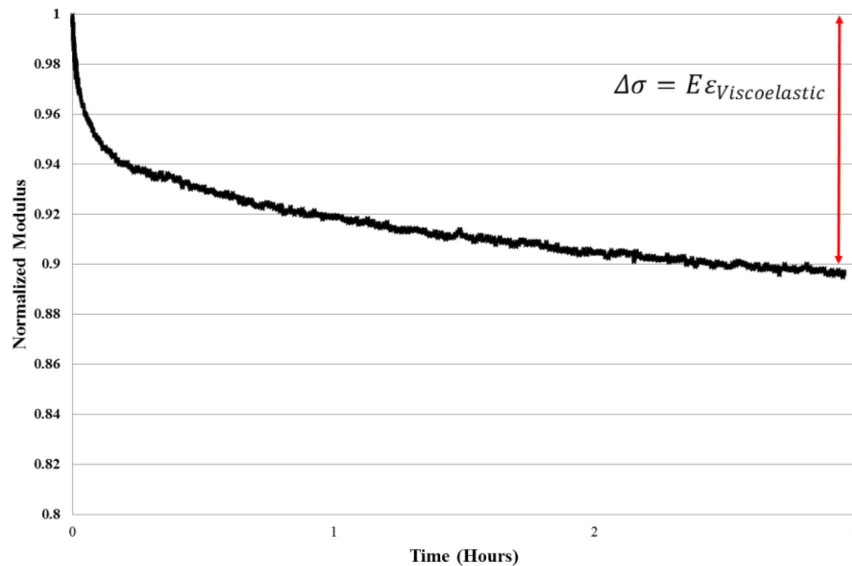

Figure 3.21 Characteristic steady state conditions at room temperature for a thin film

This simple calculation helps explain why we see no statistical difference in film behavior at room temperature when we vary ALD parameters, titanium adhesive layer

presence, or SiN_x presence. A schematic displaying the change in dislocation motion when on a free surface vs dislocation pinning on an ALD surface is shown in Figure 3.22. Even in this simple schematic, as a black stationary dislocation moves to the gray location, the viscoelastic strain value is significantly small enough that even with the presence of ALD, the dislocations only need to move several nm. The difference in line tension from dislocations being pinned by the ALD layer is negligible over a total dislocation line distance of 70.7nm

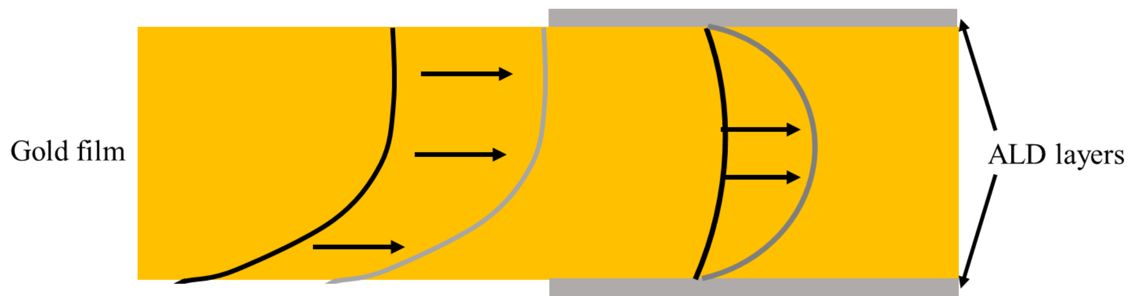

Figure 3.22 Dislocation motion without ALD coatings and with ALD coatings

Finally, a rough simulation was constructed in order to provide additional evidence that the deformation mechanism seen in this thesis is different than that seen by Lin [41]; and in turn, provide evidence as to why results in this thesis are different than seen in other stress relaxation testing conditions. Lin reported a drop in stress relaxation at elevated temperatures for thin Au films on Si cantilevers by measuring curvature change with time. Compiling the diffusion effects of the lattice, grain boundaries, dislocation cores, and plasticity from literature [51-53] allows for an initial analysis of a film response (with a given residual stress) by increasing temperature. An example of

film stress response using literature diffusion activation energies when heated to 125°C is seen in figure 3.23.

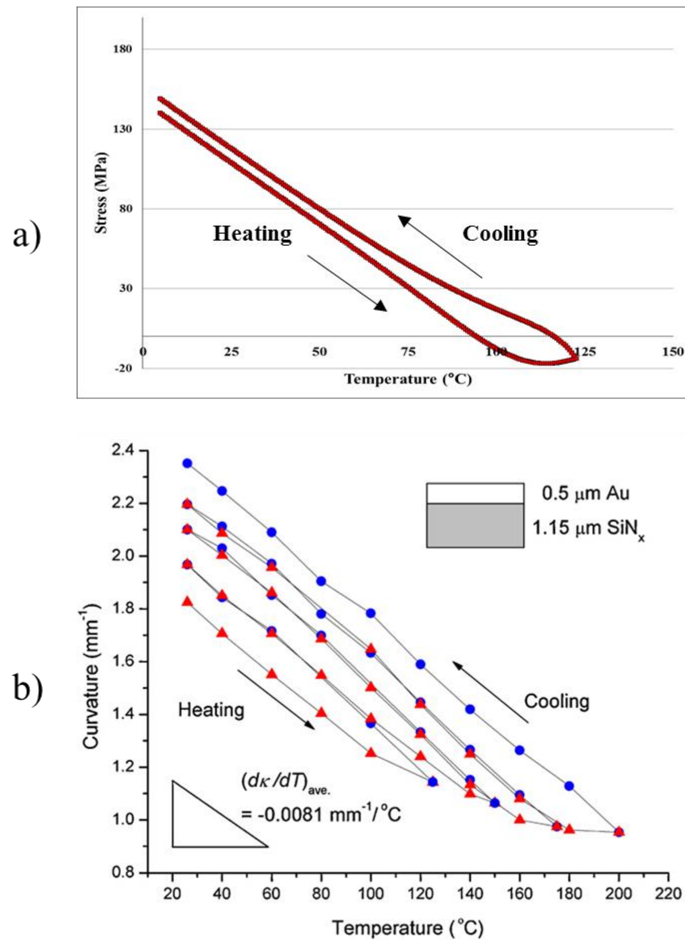

Figure 3.23 a) Plot of stress response of a material when heated past the elastic temperature limit results in an increase in residual stress results from cooling, and b) a comparison to Lin's cantilever behavior – reproduced from [41]

The simulation of a gold film stress response with temperature is Figure 3.23a. Upon heating, it is apparent that at approximately 110°C, the linear stress relationship with temperature deviates and results in stress relaxation. Once cooled, the change in stress at higher temperatures results in a larger residual stress than seen before heating. This effect is also displayed by Lin in Figure 3.23b. However, instead of just 1 temperature ramp, Lin

did 4; each showing a change in residual stress from previous conditions. Lin also noted an initial deviation from linearity at around 110°C.

Once cantilevers were coated with ALD, the degree of stress change due to temperature ramps dropped significantly, suggesting that ALD prevented a surface sensitive mechanism from allowing significant stress relaxation during temperature ramps. This is further supported by the simulation run in this thesis which shows grain boundary diffusion is the dominant deformation mechanism under these conditions. To alleviate internal stresses in a film, atoms on the surface can pass through the grain boundaries much quicker than the lattice. Lin's ALD coating effectively reduced this mechanism and resulted in less stress relaxation at higher temperatures.

Because the samples in this thesis were not affected by the presence of ALD, it has been shown that another mechanism (dislocation motion) was responsible for anelastic behavior.

3.7 Dislocation Mobility in Films

Previous work by Mongkolsuttirat [36] has shown that a double-kink dislocation theory allows for significant dislocation mobility without a relatively large activation energy. The activation energy of a kink to nucleate, W_k, can be given by [54]

$$W_k = \frac{\lambda}{\pi}(\frac{2\lambda b W_0 \sigma_p}{\pi})^{1/2} \qquad 3.3)$$

where $\lambda \approx b$ is the wavelength of the Peierls potential, which is similar to the Burgers vector b, σ_p is the Peierls stress, and $W_0 \approx \mu b^2/2$ is the line tension of the dislocation. Creating a double kink would require two kinks of equal sign to form on the same atomic plane, seen in Figure 3.24.

In this theory, a pinned dislocation in a Peierls trough must overcome the Peierls potential to reach another trough and form a kink. If this happens twice on the same dislocation a double kink (a bulged dislocation line) will form. Once created, each kink can move laterally without any required energy other than intrinsic lattice vibrations. Under stress, each kink will move laterally away from each other to alleviate applied stress (Figure 3.24b). As stated above, the total dislocation length in a grain needed to accommodate viscoelastic strain of 1.17×10^{-4} is just 70.7nm. It is not unreasonable to associate such small dislocation motion at steady state behavior to a double kink method.

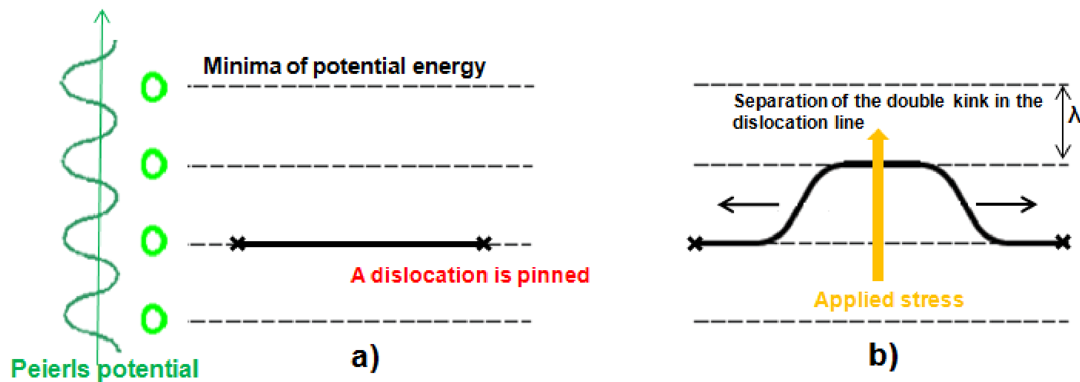

Figure 3.24 a) A dislocation segment is pinned a two points in the same Peierls energy trough, b) applying a stress causes a segment of the dislocation to advance through the Peierls potential and create a double kink.

If the applied stress is too small to cause complete dislocation glide, a time dependence behavior should result from this double kink model. As stress is applied to the film, the double kink loop will expand and result in an increase in line tension. As line tension increases, resistance to further dislocation motion develops and in turn, will increase resistance to further expansion. This decrease in rate of dislocation expansion will directly result in a decrease in stress relaxation rate.

However, when applied stress is removed, the stored energy in the dislocation line tension will bias the direction of the kinks to return to their original position. If the dislocations return to their initial state, the material will exhibit full viscoelastic recovery (steady state behavior). If the kinks have permanent displacement between their initial and final locations, the material will display viscoplastic (non-recoverable) behavior similar to the difference between initial and steady state behavior shown in experiments above. This permanent change in dislocation position could be due to unpinning from original obstacles or increased pinning from new obstacles.

Mongkolsuttirat has previously shown the estimated Peierls stress in gold to be 32 MPa, which matches well with literature values of FCC metals [55]. This assumption uses an activation energy for kink nucleation to be 0.1eV. Lytton et al [56] studied low temperature creep of single crystal pure Al, reporting an activation energy of 0.15eV. This number agrees well with previously made assumptions by Mongkolsuttirat.

4. Summary and Conclusions

The anelastic behavior of a 500nm Au film was investigated using the gas pressure bulge test method. Tests were conducted at room temperature with strains on the order of 0.1%. Varying parameters that were tested were: the presence of a Ti adhesive layer, presence of a 7.5nm Al_2O_3 ALD layer on the top and bottom surface, presence of a 200nm SiNx substrate, and presence of a 20nm TiO_2 layer on the top and bottom surface. It was observed that for samples created by identical sputtering conditions:

1) Relaxation behavior in all films had two components, one viscoelastic and one viscoplastic. Viscoelastic behavior was fully recoverable (steady state

behavior), whereas the plastic component was not. The viscoplastic behavior could also be eliminated by running subsequent iso-strain tests. This in turn conditioned the film to behave in a steady state manner.

2) Adding a 20nm titanium adhesive layer under the gold had no effect on initial or steady state behavior despite the decrease in grain size compared to pure Au tests.

3) Adding 7.5nm of Al_2O_3 to each side of the film in an attempt to mediate large reductions in time dependent modulus had no effect. Both the initial and steady state behavior were very comparable to the uncoated pure Au film and the uncoated Au/Ti film.

4) Keeping the SiN_x present during iso-strain tests also did not change the behavior of the film. The extra RIE required to remove the SiN_x will not change the initial or steady state film behavior when tested as a composite.

5) To determine if ALD thickness would change material behavior, 20nm of TiO_2 was deposited on each side of the film. There was no statistical difference in behavior for this test and other tests.

6) Calculations determined the increase in film strain due to viscoelastic contributions required an increase in dislocation line per grain of 70.1nm. If under the assumption a dislocation can span the entire grain, this number equates to <1 dislocation per grain. If under the assumption a dislocation can only span a tenth of a grain, this equates to roughly 4 dislocations needed per grain to account for viscoelastic behavior.

7) The double kink model was used to explain the time dependent behavior for films. This model also explains why the material can undergo both a viscoplastic and viscoelastic response under series of iso-strain tests.

5. References

1. Bacteria-World. *MEMS Mirror.* www.bacteria-world.com
2. SensorDynamics, Micronews. *Next Generation of MEMS gyroscopes and inertial combo sensors from SensorDynamics.* Feb 2nd, 2011.
3. G. Gregori and D. R. Clarke: *Mechanical creep as a life-limiting factor of radio frequency microswitches.* Appl. Phys. Lett. 87, 154101, 2005.
4. G. M. Rebeiz, *RF MEMS Theory, Design, and Technology.* John Wiley & Sons, 2003.
5. C. D Patel, *High Performance RF MEMS Metal-Contact Switches and Switching Networks.* Dissertation in Electrical Engineering. University of California, San Diego (2012).
6. W. D. Nix. *Mechanical properties of thin films.* Metall. Trans. A 20, 2217 (1989).
7. C. Zener. *Elasticity and Anelasticity of Metals.* University of Chicago Press. 1948.
8. X. Yan, W. L. Brown, Y. Li, J. Papapolymerou, C. Palego, J. C. M. Hwang, R. P. Vinci. *Anelastic Stress Relaxation in Gold Films and its Impact on Restoring Forces in MEMS Devices.* Journal of Microelectromechanical Systems, Vol. 18, No. 3, June 2009.
9. M. McLean, W. L. Brown, and R. P. Vinci. *Temperature-Dependent Viscoelasticity in Thin Au Films and Consequences for MEMS Devices*. Journal of Microelectromechanical Systems, Vol. 19, No. 6, December 2010.
10. S. Hyun, T. K. Hooghan, W. L. Brown, and R. P. Vinci. *Linear viscoelasticity in aluminum thin films*. Applied Physics Letters, 87, 061902 (2005).
11. W. Flugge. *Viscoelasticity.* Blaisdell Publishing Co., Massachusetts, (1975).
12. G. M. Rebeiz. *RF MEMS: Theory, Design, and Technology*. John Wiley & Sons, Inc., New York, 1st edition (2002).
13. C. Goldsmith, J. Ehmke, A. Malczewski, B. Pillans, S. Eshelman, Z. Yao, J. Brank, and M. Eberly. *Lifetime characterization of capacitive RF MEMS switches.* IEEE International Microwave Symposium, 1, 227 (2001).
14. S. T. Patton and J. S. Zabinski. *Failure mechanisms of capacitive MEMS RF switch contacts.* Tribology Letters, 19, 4, 265 (2005).
15. C. Goldsmith, J. Kleber, B. Pillans, D. Forehand, A. Malczewski, and P. Frueh, *RF MEMS: Benefits & Challenges of an Evolving RF Switch Technology*. in IEEE GaAs Dig., 147-48 (2001).
16. X. Yan. *Stress relaxation in thin Au films and associated loss of the releasing force in RF MEMS capacitive switches.* Thesis (M.S.), Lehigh University (2008).
17. K. Gall, N. West , K. Spark , M. L. Dunn , D. S. Finch. *Creep of thin film AU on biomaterial Au/Si microcantilevers.* Acta Materialia 52 (2004).
18. J.L. Loubet, W.C. Oliver, and B.N. Lucas: *Measurement of the loss tangent of low-density polyethylene with a nanoindentation technique.* J. Mater. Res. 15, 1195 (2000).

19. H. Lu, B. Wang, J. Ma, G. Huang, H. Viswanathan. *Measurememnt of creep compliance of solid polymers by nanoindentation.* Mech. Time-Depend. Mater. 7. 189 (2003).
20. W. C. Oliver and G. M. Pharr. *Measurement of hardness and elastic modulus by instrumented indentation: Advances in understanding and refinements to methodology.* J.Mater, Res 19 Vol. 1, (2004).
21. M. Hershkovitz, I. A. Blech, and Y. Komem. *Stress relaxation in thin aluminium films.* Thin Solid Films, 130, 87 (1985).
22. P. A. Gruber, S. Olliges, E. Arzt, and R. Spolenak. *Temperature dependence of mechanical properties in ultrathin Au films with and without passivation.* Journal of Materials Research, 23, 9, 2406 (2008).
23. G. G. Stoney. *Proceedings of the Royal Society of London*. A82 (553), 172 (1909).
24. Y.-L. Shen, U. Ramamurty. *Temperature-dependent inelastic response of passivated copper films. Experiment, analyses, and implications.* J. Vac. Sci. Technol. B 21, 1258 (2003)
25. Y. Zhang, M. L. Dunn, K. Gall, J. W. Elam, S. M. George *Suppression of inelastic deformation of nanocoated thin film microstructures.* Journal of Applied Physics 95, 8216 (2004).
26. B. A. Samuel and M. A. Haque. *Design and modeling of a MEMS pico-Newton loading/sensing device.* J. Micromech. Microeng. 16, 929-934 (2006).
27. D. Y. W. Yu. *Microtensile Testing of Free-standing and Supported Metallic Thin Films.* Thesis (Ph.D), Harvard University (2003).
28. D. Zhang, J-M. Breguet, R. Clavel, V. Sivakov, S. Christiansen, J. Michler. *In Situ Electron Microscopy Mechanical Testing of Silicon Nanowires Using Electrostatically Actuated Tensile Stages*. Journal of Microelectricalmechanical systems, V 19, No. 3, (2010).
29. M. McLean. *Small-scale fracture toughness studies of grain boundary embrittlement in copper-bismuth alloys* (Ph.D. Dissertation, Lehigh University, 2013).
30. J.J. Vlassak, W.D. Nix. *A new bulge test technique for the determination of Young’s modulus and Poisson’s ratio of thin films*. J. Mater. Res. 7, 3242 (1992)
31. Merle, B. *Mechanical Properties of Thin Films Studies by Bulge Testing.* (Dissertation, FAU University. 2013)
32. R. W. Balluffi, J. M. Blakely. *Special Aspects of diffusion in thin films*. Thin Solid Films, 25 (1975) 363-392
33. R.W. Balluffi, *On measurements of self-diffusion rates along dislocations in F.C.C. Metals*. Phys. Status Solidi, 42 (1970) 11
34. N.A. Gjostein. *Short circuit diffusion*. Diffusion, Am. Soc. Metals, Metals Park, Ohio, 1973, p. 241.
35. R.L.Coble. *Model for boundary diffusion controlled creep in polycrystalline materials*. J.Appl.Phys. 34, 1679 (1963).

36. K. Mongkolsuttirat. *Time and Temperature Dependence of Viscoelastic Stress Relaxation in Au and Au Alloy Thin Films* (Ph.D. Dissertation Lehigh University, 2013).
37. H. J. Frost and M. F. Ashby. *Deformation-Mechanism Maps: The Plastisity and Creep of Metals and Ceramics* Pergamon Press, Oxford, UK, (1982).
38. M. Hershkovitz, I. A. Blech, and Y. Komem. *Stress relaxation in thin aluminium films*. Thin Solid Films, 130, 87 (1985)
39. A. J. Kalkman, A. H. Verbruggen, G. C. A. M. Janssen. *Young's modulus measurements and grain boundary sliding in free-standing thin metal films.* Applied Physics Letters, 78, 18, 2673 (2001)
40. D. Gan, R. Huang, P. Ho, J Leu, J. Maiz, T. Scherban. *Effects of Passivation Layer on Stress Relaxation and Mass Transport in Electroplated Cu Films*. AIP Conference Proceedings; Vol. 741 Issue 1, p256 (2004)
41. I. K Lin, X. Zhang, Y. Zhang, *Inelastic deformation of bilayer microcantilevers with nanoscale coating.* Sensors and Actuators A: Physical 168 (2011).
42. D. Josell, F. Spaepen. *Determination of the interfacial tension by zero creep experiments on multilayers*. 1. Theory. Acta Metall Mater; 41(10):3007–15. (199)
43. K.E. Harris, A.H. King. *Direct observation of diffusional creep via TEM in polycrystalline thin films of gold*. Acta Mater; 46(17):6195–203. (1998)
44. Y. Xiang, X. Chen and J. J. Vlassak, *Plane-strain bulge test for thin films.* Journal of Materials Research 20 (09), 2360-2370 (2005).
45. J.L. Pouchou, F. Pichoir, *Surface film X-ray microanalysis*. Scanning, 12, 212. (1990)
46. M.D Groner, F.H. Fabreguette, J.W. Elam, S.M. George. *Low-temperature Al2O3 atomic layer deposition*. Chem. Mater. 16, 2004, 639-645.
47. H. Seidel, et al. *Anisotropic Etching of Crystalline Silicon in Alkaline Solutions*. J. Electrochem. Soc. Vol 137, 11, Nov 1990, 3612-3632
48. L. Zhang, J.H. Prosser, G. Feng, D. Lee. *Mechanical properties of atomic layer deposition-reinforced nanoparticle thin films*. Nanoscale. 4(20):6543-52. 2012 (supporting information)
49. W. E. Martines, G. Gregori, T. Mates. *Titanium diffusion in gold thin films*. Thin Solid Films. 518, 2585-259. 2010
50. Y. Wei, A. F. Bower, H. Gao. *Recoverable creep deformation due to heterogeneous grain-boundary diffusion and sliding*. Scripta Materialia. 57, 933-936. 2007
51. A. Ghorai, *A review on bulk diffusion in metallic solids*. diffusion-fundamentals.org, Dep. of Physics, Maulana Azad College, West Bengal, India
52. J. Mimkes, "Self-diffusion in Au along isolated dislocations." Phys. Rev. B. Vol 9, 12 (1974).
53. A. Gangulee, F.M. d'Heurle, *Activation energy for electromigration and grain boundary self diffusion in gold.* Scripta Metallurgica. Vol. 7 (1973), 1027-1030

54. G. Fantozzi, C. Esnouf, W. Benoit and I. G. Ritchie. *Internal friction and microdeformation due to the intrinsic properties of dislocations: The Bordoni relaxation*. Progress in Materials Science 27 (3–4), 311-451 (1982).
55. A. O. Moreno-Gobbi, G. Paolini and F. R. Zypman, *Peierls potential for dislocations in FCC metals.* Comp. Mat. Sci. 11 (3), 145-149 (1998).
56. S. Lytton, and Dorn, *The activation energies for creep of single aluminum crystals favorably oriented for (111) [101] slip.* Trans. Am. Inst. Mining, Met., Petrol. Engrs., 212, 220 (1958).

6. Vita

Patrick Holmes was born on March 13, 1990 to Brian and Karen Holmes in Hanover, NH. As a child he has lived in several locations in Pennsylvania, in Virginia, and as an infant in the UK. He matriculated at Lehigh University in the fall of 2008, majoring in Materials Science and Engineering. In May, 2012 he earned a B.S. in Materials Science and Engineering. He then spent 6 months as a co-op at Volvo Group Trucks Technology (where he currently works) before beginning graduate work at Lehigh in Jan, 2013, in Materials Science and Engineering.